Journal of Asian Earth Sciences 35 (2009) 469–487

Contents lists available at ScienceDirect

Journal of Asian Earth Sciences

journal homepage: www.elsevier.com/locate/jaes

Volcanological and petrological evolution of Barren Island (Andaman Sea, Indian Ocean)

Dornadula Chandrasekharam [a], Alba P. Santo [b,c,*], Bruno Capaccioni [d], Orlando Vaselli [b,c], Mohammad Ayaz Alam [a], Piero Manetti [b], Franco Tassi [b]

[a] Department of Earth Sciences, Indian Institute of Technology Bombay, 400076 Mumbai, India
[b] Department of Earth Sciences, Via G. La Pira, 4, 50121 Florence, Italy
[c] CNR-IGG Institute of Geosciences and Earth Resources, Via G. La Pira, 4, 50121 Florence, Italy
[d] Department of Earth and Geological-Environmental Sciences, Piazza Porta San Donato, 1, 40126 Bologna, Italy

ARTICLE INFO

Article history:
Received 19 September 2008
Received in revised form 11 February 2009
Accepted 24 February 2009

Keywords:
Barren Island
Field volcanology
Petrology
Radiogenic isotopes
Fluid geochemistry

ABSTRACT

The Island of Barren (Andaman Sea, Indian Ocean) consists of a horseshoe-shaped caldera opened to the west that was formed by either a giant, lateral landslide of the original volcanic cone or a vertical collapse of a surficial magma chamber due to a paroxysmal eruption. The reconstruction of the pre-and post-caldera activity indicates that the subaerial volcanic history of Barren Island was characterized by effusive activities accompanied by subordinate explosive (scoria fall) eruptions. The collapse of the central portion of the edifice terminated this mainly effusive phase. The inner flanks and the rim of the depression are covered by a 20 m thick sequence of breccias and tuffs. Beds are structurally massive with steep fronts, likely due to secondary mass flowage. The lack of caldera-forming eruption together with the absence of chemically evolved magmas could suggest a lateral landslide as the most probable process responsible for the caldera formation. The active polygenic tuff cone, presently occupying the inner portion of the caldera, consists of at least five coalescent summit craters and four eccentric spatter cones at the base. These features are attributed to the historic activities that are dominated by the emplacement of lava flows and pyroclastic deposits (e.g. 1803, 1991, 1995 and, possibly, 2000 eruptions). Lava flows moved westward from lateral spatter cones and occasionally reached the sea. A few months after the 2004 tsunami and Sumatra earthquake, Barren Island volcano violently resumed its eruptive activity that lasted for almost two years. The volcanic products ejected from May 2005 eruption have covered the historic lava flows and pyroclastic deposits.

Petrologically, the lava flows show a narrow compositional variation, from low-K basalts to basaltic andesites. Pre-caldera magmas display a general less evolved composition and a certain variability of the Sr isotopic ratios (0.70385–0.70400); post-caldera magmas are compositionally more homogeneous and have an almost constant Sr isotopic ratio (0.70399–0.70403). Petrographic and geochemical characteristics indicate an important role played by a crystal–liquid fractionation process. However, the presence of large phenocrysts of xenocrystic origin, the small but significant variations of Sr isotopic ratios in the pre-caldera magmas, the relationships between $^{87}Sr/^{86}Sr$ and trace elements and the ratios of incompatible trace elements in the basaltic rocks point to the occurrence of additional evolutionary processes and/or to a role of a heterogeneous magma source. The most primitive magma (Mg# 71, Ni 218 ppm, Cr 557 ppm), displaying the lowest Th content (0.39 ppm), found in the Barren Island is also the most primitive in the Burma-Andaman-Java Arc, thus representing an important reference composition for the region.

1. Introduction

Barren (12.29°N, 93.85°E, Andaman Sea, Indian Ocean) and Narcondam are two subduction-related volcanic islands lying about 135 and 270 km ENE of Port Blair (the capital of the Andaman and Nicobar Archipelago) (Fig. 1). Barren Island (hereafter, BI) (ca. 10 km^2) represents the only active volcanic system in the Indian subcontinent, the last event occurring a few months after the great earthquake of Sumatra (December 26, 2004; e.g. Francke et al., 2008 and references therein). Narcondam volcano has no record of activity in the recent times but it appears to have erupted in the Holocene (Simkin and Siebert, 1994). Besides the dormant vol-

* Corresponding author. Address: Department of Earth Sciences, Via G. La Pira, 4, 50121 Florence, Italy. Tel.: +39 055 2757503; fax: +39 055 290312.
E-mail address: alba.santo@unifi.it (A.P. Santo).

1367-9120/$ - see front matter © 2009 Elsevier Ltd. All rights reserved.
doi:10.1016/j.jseaes.2009.02.010

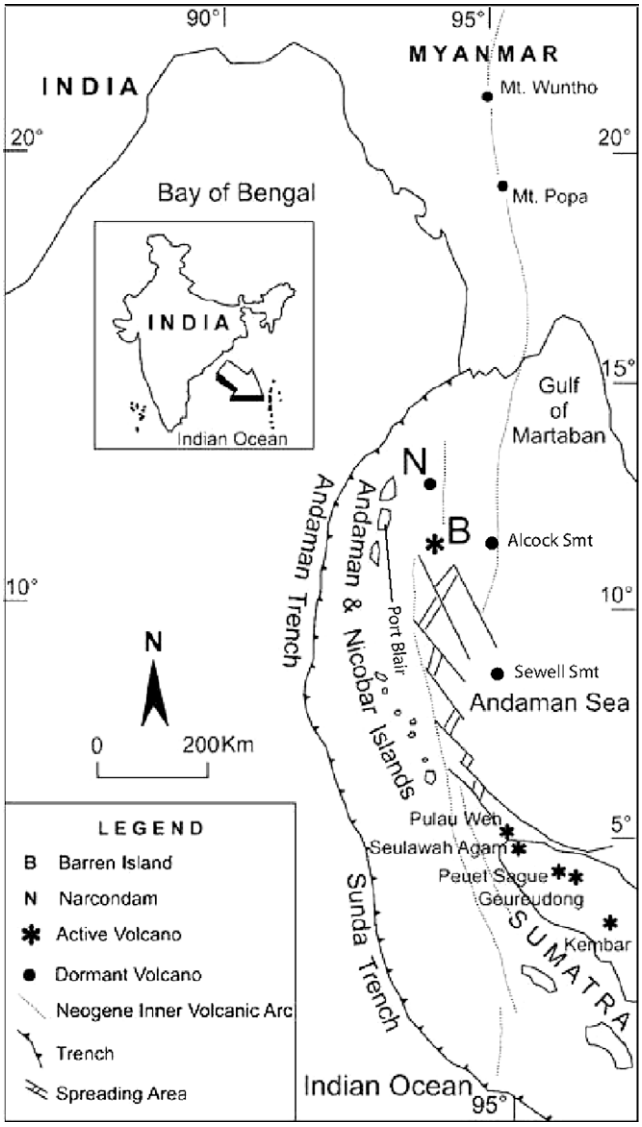

Fig. 1. Barren Island on Myanmar–Andaman–Sumatra volcanic arc (modified after Rodolfo, 1969).

cano of Narcondam, there are also a few volcanic seamounts in the neighboring region of the Andaman Sea, viz. Alcock SMT, about 60 km east of Barren Island and Sewell SMT, about 200 km east of Car Nicobar (Fig. 1).

BI rises for about 2300 m from the sea floor, with an elevation of 355 m a.s.l. The oldest rocks are apparently related to the Late Pleistocene, although no radiometric ages are available. The juvenile products are generally referred to basalt and basaltic andesites (e.g. Alam et al., 2004; Luhr and Haldar, 2006) and differ from those emitted in Narcondam, where porphyritic dacite, amphibole-andesite and andesite dominate (Pal et al., 2007a). Several eruptions have occurred in the historic times: 2005, 2000 (?), 1994–95, 1991, 1852(?), 1803–04, 1795, 1789 and 1787 (e.g. Hobday and Mallet, 1885; Ball, 1888, 1893; Mallet, 1895; Washington, 1924; Haldar, 2001; Haldar and Luhr, 2003; Alam et al., 2004; Luhr and Haldar, 2006; Pal et al., 2007b). After about 140 years of quiescence, the volcanic activity of BI has resumed in 1991 with explosive events frequently coupled with the emission of lava flows that have reached the sea. These different explosive and effusive episodes were likely emitted from the intra-calderic polygenetic volcanic edifice presently occupying the central-western part of the

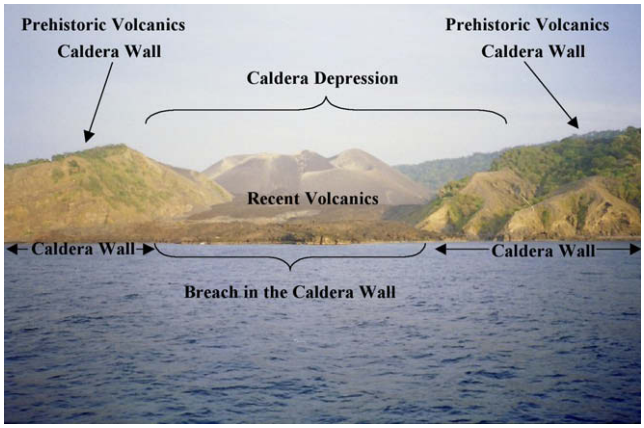

Fig. 2. View of Barren Island in February 2003 from West showing the caldera wall flanking the recent volcanics and the breach in the caldera wall through which flows of recent eruptions have reached the sea.

island (Fig. 2). In this paper, we present the results deriving by a volcanological study and new chemical and isotopic ($^{87}Sr/^{86}Sr$ and $^{143}Nd/^{144}Nd$) data obtained from different lava flows belonging to both pre-calderic and historical events with the aims to (i) reconstruct the volcanic sequence and the petrological evolution of the island, (ii) identify the causes of the calderic collapse and (iii) propose a new geological map by modifying those of Haldar et al. (1992a) and Haldar and Luhr (2003).

2. Tectonic setting

Barren and Narcondam islands are the emerged lands of a part of the inner arc of Burma-Andaman-Java subduction complex (e.g. Mitchell, 1985). The importance of BI cannot be overstated, as it is the last of the active volcanoes towards the northern part of the volcanic arc, named as Neogene Inner Volcanic Arc (NIVA) by Haldar et al. (1992a,b,c) and the southeastern Asian Volcanic Rim (Evans and Crompton, 1946). The NIVA extends from the dormant volcanoes of Myanmar (e.g. Popa, Wuntho, e.g. Maury et al., 2004 and references therein) to those of active Sunda and Banda Arc (e.g. Wheller et al., 1987) and runs almost sub-parallel to and 100–130 km east of Arakan Yoma, Andaman-Nicobar and Sumatran ophiolite belts followed by easterly dipping subduction zone. To the north, this volcanic arc merges with the Himalayan collision

Fig. 3. Central polygenetic cinder cone with lateral spatter cones as seen from the southern part of Barren Island (photo taken in February 2003).

zone, while to SE it joins the Pacific Ring of Fire. Location of BI is quite unique since it is located in a region where collision (without subduction) and subduction are concurrent because of the oblique convergence (Fitch, 1972; Curray et al., 1979) of the Indian and Burmese plates. Arc volcanic activities in the Mesozoic and Cenozoic Eras have been reported from Burma and Sumatra (Mitchell, 1985). According to Banerjee and Shaw (2001), the volcanic arc is a Cretaceous fold belt associated with discontinuous submarine ridge of andesite effusive volcanic sea highs, which can be traced from the Central Molasse Basin of Myanmar through Narcondam and BI into the structural trend of Sumangko rift zone, along the volcanic Barisan axis of northern Sumatra. This volcanic arc is believed to have evolved as a result of eastward subduction of the Indian Ocean lithosphere below the SE Asian plate. Oblique convergence (Fitch, 1972; Curray et al., 1979) between the Indo-Australian plate and the Indo-Myanmar–Andaman–Sumatra block has developed a subduction regime, a volcanic arc and an easterly dipping Benioff zone along the western margin of this block. Moreover, the distribution of earthquakes in the Burmese Arc region suggests the presence of a subducted Indian lithospheric slab beneath the Burmese plate (Verma et al., 1976; Mukhopadhyay and Dasgupta, 1988; Ni et al., 1989; Gupta et al., 1990). The nature of convergence varies from a continental type in the Burmese Arc to an oceanic type in the Andaman–Nicobar Arc, with a relatively ase-

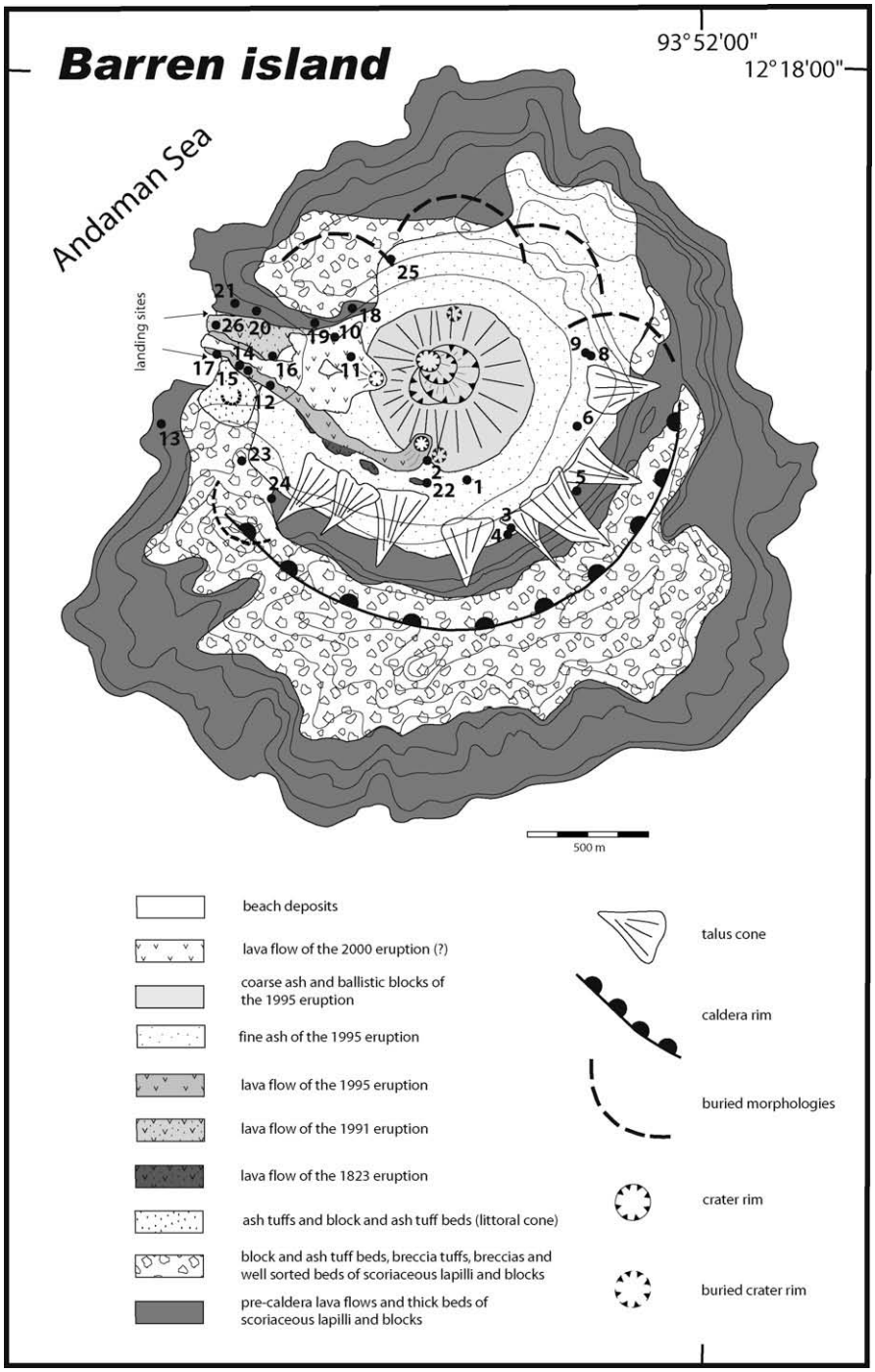

Fig. 4. Geological map of Barren Island based on the field mapping carried out in February 2003. Topographic contours are from Haldar (1989).

ismic zone marking the transition (Chandra, 1984). Shallow and occasional intermediate-depth earthquakes delineate the subducted slab under the Andaman-Nicobar islands joining the seismicity trend of the Indo-Burmese ranges. A distinct separate lineation of shallow focus earthquakes passes under the Central Basin of the Andaman Sea and indistinctly follows the line of the Sagiang Fault towards the eastern Himalayan syntaxis (Curray et al., 1979). Active subduction of the Indian lithosphere below the Burma plate is primarily evidenced by the presence of: (i) the Barren–Narcondam active volcanic arc that continues to the continental margin arc in Sumatra (Rodolfo, 1969); (ii) the correlation of the Andaman Arc-trench bathymetry to morphotectonic elements and their underlying seismic zones (Dasgupta and Mukhopadhyay, 1993); (iii) the eastwardly dipping Benioff zone defined by earthquakes of up to 200 km focal depth (Mukhopadhyay, 1984); (iv) the anomalous heat flow pattern (Burns, 1964; Closs et al., 1974; Curray et al., 1982); and (v) the large amplitude bipolar gravity field characteristic of the subduction zones (Mukhopadhyay and Krishna, 1991). Major tectonic features along the arc are the Indo-Burmese ranges to the north and the Andaman–Nicobar ridge to the south. The Sumatran fault (Semangko fault) system in the southeast, the Western Andaman fault and Sagaing fault (Myanmar) further east are the features supporting major right lateral movements in this region (Bhatia et al., 1999). The Neogene Andaman back-arc spreading ridge (Dasgupta and Mukhopadhyay, 1993) is related to oblique convergence of the Indian plate against the Asian continental margin, where actual spreading occurred possibly through the leaky transform (Eguchi et al., 1979; Uyeda and Kanamori, 1979).

3. Physiography

Barren Island/BI is uninhabited by humans. A small population of goats, birds, bats (flying foxes) and a few rodent species (rats), whose life is supported by the thick vegetation all over the caldera wall and freshwater springs within the ash beds (Chandrasekharam et al., 2003), lives in.

The volcano consists of a 2 km-wide caldera, open towards the west, with inner walls up to 250 m high (Figs. 2 and 3), which could have been formed either by a giant, non-eruptive lateral landslide of the original volcanic cone or by vertical collapse of a surficial magma chamber as a result of a paroxysmal eruption and an intra-calderic, polygenetic tuff cone. The elevation of the prehistoric cone, the collapse of which resulted in the formation of caldera, has been estimated to be about 1100 m from the ocean floor, with its base having a diameter of about 12 km, taking into consideration the outer slope of the caldera wall (~30°) and the present sub-aerial diameter (3.5 km) of the island (Bandyopadhyay et al., 1973; Raina, 1987). The inner part of the caldera is occupied by an active, 305 m high, polygenetic tuff cone (Fig. 2).

Historic and recent volcanic activities are confined within the caldera depression, whereas the caldera wall represents the prehistoric volcanism. At least four spatter cones occur, located on the western, southern and southeastern flanks of the central cone. Lava flows have covered most of the western part of the caldera floor and have reached the sea during eruptions in the 19th century and more recently in 1991, 1995, 2000(?) and 2005. As previously mentioned, the first recorded eruptions of the volcano date back to 1787. Since then the volcano has erupted at least 7–8 times: 1789, 1795, 1803–04, 1832, and, after a 140 year long dormant period, 1991 and 1994–95. The latter is probably the most well described activity occurred in the island (e.g. Haldar et al., 1999; Haldar and Luhr, 2003). It is worthwhile to mention that, according to visual shipboard observations taken from about 0.8 km offshore of Barren Island, the Indian Coast Guard reported renewed activities (strong gas and possible lava emissions) in January 2000. Ash plumes and lava flows were described since May 2005–January 2006 (e.g. BGVN, 2005, 2006). A compilation of MODIS thermal anomaly data from the Aqua and Terra satellites suggests that the 2005 event began on 26 May 2005 (BGVN, 2006) and has likely continued through 1 September 2007.

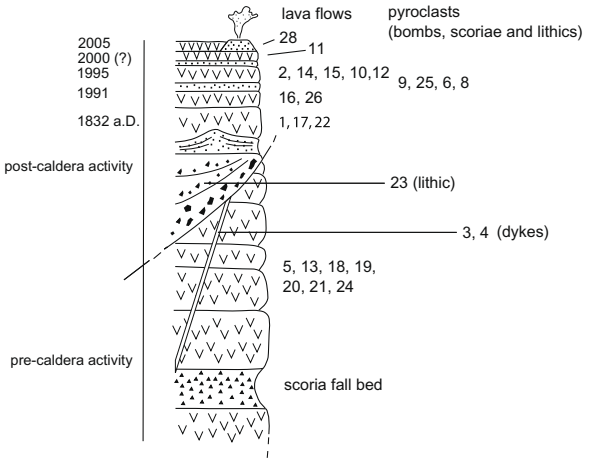

Fig. 5. Schematic stratigraphical column showing the main volcanic events that have concurred to the evolution of Barren Island. Numbers indicate the samples collected for chemical and isotopic analysis.

Fig. 6. Scoria fall beds, affected by normal faults, along the base of the caldera walls.

Fig. 7. Caldera wall in the western part of Barren Island where at least six lava flows can be recognized.

4. General outlines of the volcanic evolution of the island

A detailed geological map has resulted from the fieldwork carried out in February 2003 and is presented in Fig. 4 by using the topographic contours of Haldar (1989), whilst a schematic startigraphic column is shown in Fig. 5.

The sub-aerial volcanic history of BI commenced with effusive activities, as testified by a sequence of lava flows up to 3 m thick, cropping out along the inner flanks of the caldera, and subordinate explosive eruptions, mostly producing scoria fall beds, dislocated across the bedding planes (Fig. 6). At least six lava flows can be recognized along the northern part of the caldera (Fig. 7). The pre-caldera activity also witnessed the intrusion of a dyke (Alam et al., 2004) along the southern part of the caldera. This mainly effusive phase ended with the collapse of the central portion of the edifice. As reported in Figs. 2 and 4, the resulting depression, now occupying the largest portion of the island, has a westward-opened horseshoe-shaped morphology. With the interposition of a well-defined angular unconformity, the inner flanks and the rim of the depression are directly covered by a sequence of breccias and tuffs up to 20 m thick. The sequence appears as a monotonous piling up of thick beds of blocks and lapilli breccias and tuffs composed by angular shaped black lavas supported in a pale yellow ash matrix (Fig. 8). Beds are structurally massive and, where visible, display steep fronts, likely suggesting to be the result of secondary mass flowage. Close to the base of the sequence, a single bed of well-sorted scoriaceous lapilli and blocks can be identified. A local sequence of tuffs, possible pertaining to a local small tuff cone, crops out very close to the open-to-sea sector with an apparent thickness of 6 to 8 m. This sequence appears to be composed of thick laminae to thin beds of tuffs and lapilli tuffs, frequently showing gas vesiculation and soft sediment deformations. Impact sags with angular blocks of black lavas are also common. As mentioned, in February 2003 the inner portion of the collapsed area was occupied by an active polygenic tuff cone, consisting of at least five coalescent summit craters and four eccentric spatter cones located south, west and north with respect to the main edifice. These morphologies can be related to the historic activities documented since the 1787 eruption (Siebert and Simkin, 2002), although no clear evidence of volcanic deposits older than the 1803 lava flow has been recognized. The historic activity, which occurred entirely within the caldera depression, appears to be characterized by the emplacement of lava flows and pyroclastic deposits. Lava flows are related to 1787(?), 1803, 1832, 1991, 1995 and, possibly,

Fig. 8. Thick bed of block and lapilli breccia covering the caldera inner wall.

Table 1
Representative microprobe analyses of minerals (in wt. %) from Barren Island.

Plagioclase

	Pre-caldera																							
	BAR 24			BAR 13	BAR 18				BAR 19		BAR 5			BAR 3				BAR 4					
	Ph core	Ph rim	Mph core	LPh core	Ph core	Ph rim	Mph core	Gdm	LPh core	Ph rim	LPh core	Ph rim	Ph core	LPh core	Ph rim	Mph core	Gdm	Ph core	Ph rim	Ph core	Ph rim	Mph core	Gdm
SiO_2	46.8	48.9	46.3	44.9	46.7	47.9	43.8	48.2	46.3	50.7	44.7	50.7	49.7	45.4	49.8	49.9	51.6	46.4	47.2	46.1	50.3	46.2	51.1
Al_2O_3	33.7	33.0	34.3	35.2	33.0	33.1	34.9	31.5	34.6	32.0	35.0	31.1	31.9	34.5	31.1	31.7	30.4	33.9	33.6	34.6	32.0	34.0	30.9
FeO_{tot}	0.57	0.61	0.69	0.48	0.84	0.63	0.48	0.67	0.53	0.55	0.63	0.64	0.6	0.47	1.05	0.68	0.97	0.49	0.67	0.52	0.88	0.74	0.87
CaO	17.5	16.3	18.4	18.4	17.0	16.5	18.8	15.4	18.3	15.0	18.2	14.1	14.9	18.8	14.8	14.7	13.6	17.8	17.6	18.3	14.9	18.1	14.3
Na_2O	1.42	2.41	1.2	0.68	1.59	1.93	0.67	2.61	1.07	2.98	0.76	3.37	2.91	0.91	3.12	2.65	3.51	1.31	1.63	1.13	2.95	1.21	3.26
K_2O	0.02	0.03	–	0.03	–	0.04	–	0.07	–	0.05	0.03	0.07	0.11	–	0.09	0.05	0.09	0.03	0.01	0.03	0.15	0.04	0.14
Total	100.1	101.2	100.8	99.7	99.2	100.1	98.7	98.4	100.7	101.3	99.3	100.0	100.0	100.2	100.0	99.7	100.2	100.0	100.8	100.7	101.1	100.2	100.5
An %	87.1	78.8	89.4	93.6	85.5	82.4	93.9	76.2	90.4	73.4	92.8	69.5	73.4	91.9	72.0	75.1	67.9	88.1	85.6	89.8	72.9	89.0	70.2
Ab %	12.8	21.1	10.6	6.3	14.5	17.4	6.1	23.4	9.6	26.4	7.0	30.1	26.0	8.1	27.5	24.6	31.6	11.7	14.3	10.1	26.2	10.8	28.9
Or %	0.12	0.17	–	0.18	–	0.24	–	0.41	0.00	0.29	0.18	0.41	0.65	–	0.52	0.31	0.53	0.18	0.06	0.18	0.88	0.23	0.82

	Pre-caldera lithic				Post-caldera					Post-caldera								
					1787–1832					*1991*								
	BAR 23				BAR 1					BAR 6				BAR 16		BAR 26		
	Ph core	Ph rim	Mph core	Gdm	Ph core	Ph rim	LPh core	Ph rim	Mph core	Ph core	Ph rim	Mph core	Gdm	LPh core sieved	Ph rim	Ph core	Ph rim	Gdm
SiO_2	44.4	52.2	55.2	54.0	48.1	49.7	45.0	51.5	45.9	46.9	52.0	49.1	51.8	45.4	50.7	46.1	51.2	56.4
Al_2O_3	34.0	29.4	28.9	28.4	33.0	32.1	35.5	30.9	33.9	33.5	30.2	31.9	29.0	35.9	31.5	35.0	30.7	26.6
FeO_{tot}	0.44	1.02	0.93	0.77	0.84	0.79	0.36	0.61	0.59	0.51	0.88	0.73	0.88	0.48	0.68	0.49	0.71	1.04
CaO	18.2	12.1	11.0	11.1	16.6	14.9	18.9	14.2	17.3	16.7	13.1	15.1	12.7	18.8	14.3	18.0	13.9	9.1
Na_2O	1.01	4.3	5.02	4.96	2.12	2.82	0.68	3.58	1.54	1.61	3.64	2.73	3.86	0.73	3.32	1.12	3.52	6.23
K_2O	0.02	0.16	0.12	0.13	0.06	0.04	–	0.08	–	0.04	0.04	0.09	0.08	0.05	0.06	–	0.08	0.26
Total	98.1	99.2	101.1	99.4	100.7	100.4	100.5	100.8	99.2	99.3	99.9	99.6	98.4	101.4	100.5	100.7	100.1	99.6
An %	90.8	60.3	54.4	54.9	81.0	74.3	93.9	68.3	86.1	84.9	66.4	74.9	64.2	93.2	70.2	89.9	68.2	44.0
Ab %	9.1	38.7	44.9	44.4	18.7	25.5	6.1	31.2	13.9	14.8	33.4	24.5	35.3	6.5	29.5	10.1	31.4	54.5
Or %	0.12	0.95	0.71	0.77	0.35	0.24	–	0.46	–	0.24	0.24	0.53	0.48	0.29	0.35	–	0.47	1.50

	Post-caldera																			Lithic	
	1995–2000																				
	BAR 10		BAR 11					BAR 14						BAR 15					BAR 12			BAR 9	
	LPh core	Ph rim	Lph core	Lph rim	Mph core	Mph rim	Gdm	LPh core	Mgph rim	LPh core	Ph rim	Mph core	Mph rim	LPh core	Ph rim	Mph core	Mph rim	Gdm	LPh core	Ph rim	Gdm	Ph core	Mph core
SiO_2	45.3	52.4	45.1	52.1	47.2	46.7	53.6	44.9	51.2	44.8	47.0	45.5	51.2	44.4	45.4	46.4	51.8	52.0	44.4	46.1	47.4	48.2	48.1
Al_2O_3	34.8	30.3	35.0	30.1	34.0	28.8	28.7	34.9	30.9	35.8	33.7	34.5	30.5	35.8	35.4	34.3	30.4	30.0	35.1	34.0	34.0	33.3	33.6
FeO_{tot}	0.6	0.79	0.6	0.79	0.64	0.84	1.2	0.53	0.74	0.37	0.81	0.49	0.77	0.4	0.48	0.74	0.85	0.76	0.34	0.63	0.67	0.29	0.32
CaO	18.2	13.3	18.3	13.2	17.1	14.0	11.8	18.7	13.9	19.2	17.2	18.6	14.0	18.9	18.2	17.5	13.2	12.9	18.7	17.6	17.8	15.7	16.1
Na_2O	0.99	3.93	0.89	3.98	1.57	3.29	4.76	0.74	3.53	0.6	1.53	0.67	3.38	0.56	0.79	1.34	3.65	3.65	0.79	1.39	1.44	2.2	1.95
K_2O	–	0.09	0.05	0.02	–	0.02	0.15	0	0.1	0.02	0.03	–	0.04	–	–	0.04	0.09	0.06	–	0.01	–	–	–
Total	99.9	100.8	100.0	100.1	100.4	93.6	100.2	99.9	100.3	100.9	100.3	99.7	99.9	100.0	100.3	100.3	100.1	99.3	99.3	99.8	101.4	99.7	100.1
An %	91.0	64.9	91.6	64.5	85.7	70.1	57.3	93.3	68.0	94.5	86.0	93.9	69.4	94.9	92.7	87.6	66.3	65.8	92.9	87.4	87.3	79.8	82.0
Ab %	9.0	34.6	8.1	35.3	14.3	29.8	41.9	6.7	31.4	5.3	13.8	6.1	30.3	5.1	7.3	12.1	33.1	33.8	7.1	12.5	12.7	20.2	18.0
Or %	–	0.52	0.30	0.12	–	0.12	0.87	0.00	0.59	0.12	0.18	–	0.24	–	–	0.24	0.54	0.37	–	0.06	–	–	–

Clinopyroxene

	Pre-caldera																					Lithic		
	BAR 24			BAR 13		BAR 18			BAR 19			BAR 5				BAR 3				BAR 4			BAR 23		
	Ph core	Mph core	Gdm	Mph core	Gdm	Ph core	Ph rim	Gdm	Ph core	Ph rim	Gdm	Ph core	Ph rim	Mph core	Gdm	Ph core	Ph rim	Mph core	Gdm	Ph core	Mph core	Gdm	Ph core	Ph rim	Gdm
SiO_2	51.0	51.3	51.7	50.3	49.6	51.1	51.0	50.8	51.3	49.6	52.6	50.2	51.6	50.7	51.1	51.6	51.8	51.7	50.8	52.0	51.1	52.2	50.2	51.1	52.3
TiO_2	0.58	0.5	0.75	0.54	0.93	0.68	0.55	0.88	0.58	1.02	0.54	0.52	0.5	0.59	0.71	0.5	0.49	0.37	0.76	0.4	0.58	0.55	0.75	0.62	0.42
Al_2O_3	4.9	3.7	2.8	4.7	3.1	3.1	2.7	2.8	3.4	3.1	1.6	4.9	2.6	2.4	1.5	3.4	3.0	3.0	3.6	4.1	3.3	2.1	3.1	2.8	0.4
Cr_2O_3	0.61	0.37	0.09	0.24	0.3	–	0.02	0.02	0.56	0.06	0.12	0.34	0.08	–	0.05	0.56	0.57	0.61	0.44	0.45	0.08	0.13	0.29	0.16	0.05
FeO_{tot}	5.5	6.6	8.4	6.2	14.0	8.0	8.6	11.2	6.4	9.9	10.0	5.5	7.9	8.6	11.6	6.1	4.8	5.0	7.0	4.4	7.3	9.0	7.6	9.4	23.2
MnO	0.15	0.15	0.38	0.08	0.46	0.32	0.32	0.3	0.17	0.25	0.45	0.23	0.33	0.33	0.48	0.25	0.13	0.17	0.23	0.17	0.35	0.36	0.22	0.28	0.87
MgO	15.3	15.6	16.4	15.2	13.6	15.2	15.3	16.0	16.2	14.6	16.8	15.8	16.1	16.1	15.5	15.4	16.2	16.3	15.2	16.0	14.7	16.6	14.5	16.2	18.4
CaO	22.3	21.0	18.2	22.3	16.4	21.0	20.5	17.5	21.2	19.8	18.1	22.8	20.6	20.4	17.7	21.9	22.8	22.5	20.7	22.7	21.4	17.7	22.9	19.0	4.1
Na_2O	0.25	0.36	0.31	0.19	0.43	0.2	0.29	0.38	0.27	0.28	0.22	0.24	0.23	0.26	0.31	0.25	0.25	0.24	0.37	0.14	0.36	0.42	0.42	0.36	0.1
Total	100.5	99.7	98.9	99.6	98.9	99.5	99.4	100.0	100.1	98.6	100.4	100.4	99.9	99.4	98.9	100.0	100.1	99.9	99.2	100.4	99.1	99.0	100.0	99.9	99.8
Wo%	46.4	43.8	37.9	46.2	35.1	43.2	42.0	35.8	43.4	41.2	36.5	46.3	41.6	40.9	36.4	45.4	46.4	45.6	43.6	46.8	44.7	36.7	46.5	38.7	8.4
En%	44.4	45.2	47.6	43.7	40.6	43.4	43.7	45.7	46.2	42.3	47.0	44.6	45.3	45.1	44.3	44.4	45.8	46.2	44.6	45.9	42.8	48.1	41.1	45.9	52.9
Fs%	9.2	11.0	14.4	10.1	24.3	13.4	14.3	18.5	10.4	16.5	16.5	9.1	13.0	14.0	19.3	10.2	7.8	8.2	11.9	7.4	12.5	15.1	12.4	15.4	38.7
Mg#	83.3	80.7	77.6	81.4	63.4	77.2	76.0	71.8	81.9	72.5	74.9	83.6	78.4	77.0	70.5	81.9	85.7	85.4	79.5	86.6	78.2	76.8	77.3	75.4	58.6

	Post-caldera																				Lithic		
	1787–1832		*1991*						*1995–2000*														
	BAR 1		BAR 6		BAR 16	BAR 26			BAR 10				BAR 11	BAR 14		BAR 15	BAR 12				BAR 9		
	Ph core	Mph core	Ph core	Ph rim	Gdm	Ph core	Ph rim	Gdm	Ph core	Ph rim	Mph core	Gdm	Gdm	Ph core	Gdm	Gdm	Ph core	Ph rim	Mph core	Gdm	Ph core	Ph core	Ph core
SiO_2	48.7	52.1	51.2	50.0	52.2	49.1	51.3	52.8	51.7	52.0	50.6	52.2	50.5	52.3	50.9	53.8	51.0	51.3	50.4	52.9	53.6	53.4	53.3
TiO_2	0.84	0.45	0.61	0.79	0.44	1	0.57	0.3	0.61	0.52	0.87	0.41	0.88	0.49	0.78	0.28	0.82	0.78	0.94	0.8	0.64	0.68	0.77
Al_2O_3	3.9	1.6	3.2	3.8	0.7	4.2	1.9	0.5	2.1	2.0	2.3	1.8	3.4	1.9	2.3	0.7	3.3	3.8	2.6	3.0	1.3	1.5	1.7
Cr_2O_3	0.03	0.06	–	0.05	–	–	0.03	–	–	0.08	–	0.11	0.2	0.06	0.22	–	–	–	0.06	–	0.03	0.16	0.13
FeO_{tot}	8.3	11.3	8.3	8.7	21.0	9.3	9.7	21.6	9.6	9.3	11.0	9.3	10.4	8.0	12.8	19.8	8.7	8.1	11.2	15.0	5.6	5.8	6.0
MnO	0.26	0.48	0.29	0.27	0.67	0.4	0.35	0.78	0.31	0.4	0.38	0.3	0.27	0.43	0.53	0.49	0.45	0.22	0.35	0.61	0.09	–	–
MgO	14.5	17.5	15.5	14.8	18.7	14.5	16.2	20.4	14.9	16.7	15.2	16.5	15.1	16.3	15.5	22.6	15.1	14.3	14.7	13.5	17.3	16.1	15.9
CaO	21.4	15.3	20.9	21.3	6.4	20.1	18.4	3.8	19.9	18.9	19.1	18.7	19.2	20.8	16.6	4.0	20.5	21.1	18.7	13.8	22.0	21.8	21.4
Na_2O	0.33	0.24	0.35	0.28	0.21	0.35	0.2	0.04	0.22	0.21	0.32	0.31	0.26	0.37	0.36	0.07	0.32	0.33	0.39	0.66	0.38	0.45	0.38
Total	98.2	99.0	100.3	99.9	100.4	99.0	98.7	100.2	99.3	100.1	99.8	99.6	100.1	100.6	99.9	101.8	100.2	100.0	99.4	100.3	100.8	99.9	99.4
Wo%	44.3	31.3	42.4	43.6	12.9	42.1	37.8	7.7	41.1	38.0	38.8	38.0	39.6	41.5	34.2	7.7	42.1	44.4	38.8	30.8	43.6	44.7	44.4
En%	41.9	49.8	44.0	42.1	52.7	42.2	46.1	57.1	42.9	46.7	43.0	46.7	43.3	45.3	44.4	61.4	43.2	42.0	42.5	41.9	47.7	46.0	45.9
Fs%	13.8	18.9	13.6	14.3	34.3	15.8	16.1	35.2	16.0	15.3	18.2	15.3	17.1	13.2	21.4	30.9	14.7	13.6	18.7	27.2	8.8	9.3	9.7
Mg#	75.8	73.4	77.0	75.2	61.3	73.6	74.8	62.7	73.4	76.1	71.0	75.9	72.2	78.3	68.3	67.0	75.5	76.0	70.1	61.6	84.7	83.1	82.6

Olivine

	Pre-caldera																		Lithic	
	BAR 24		BAR 13		BAR 18		BAR 19			BAR 5			BAR 3			BAR 4			BAR 23	
	Ph core	Mph core	Ph core	Ph rim	Ph core	Ph rim	Ph core	Ph rim	Mph core	Ph core	Ph rim	Mph core	Ph core	Ph rim	Mph core	Ph core	Mph core	Gdm	Ph core	Mph core
SiO_2	40.3	40.5	39.2	38.5	39.0	38.2	37.6	37.4	37.6	38.3	36.6	35.8	40.5	38.6	39.2	38.9	38.4	38.0	37.5	37.4
FeO_{tot}	15.9	15.9	21.0	24.9	19.6	24.1	21.7	26.1	27.2	19.7	25.2	29.2	13.0	23.3	20.0	22.2	22.4	26.1	27.4	27.0
MnO	0.32	0.31	0.38	0.51	0.33	0.36	0.38	0.5	0.51	0.28	0.51	0.43	0.29	0.44	0.39	0.46	0.58	0.56	0.54	0.55
MgO	43.7	44.3	40.8	38.2	42.7	39.1	40.7	36.7	35.4	41.0	36.0	32.5	46.4	37.3	40.6	38.2	37.5	34.7	35.2	35.8
CaO	0.16	0.18	0.2	0.16	0.12	0.21	0.16	0.17	0.2	0.26	0.19	0.17	0.12	0.28	0.26	0.16	0.22	0.24	0.21	0.17
Cr_2O_3	–	0.12	0.01	–	0.07	0.06	0.07	0.05	–	–	–	0.04	0.09	–	–	–	–	–	0.07	0.05
Total	100.4	101.4	101.5	102.3	101.8	102.1	100.6	100.9	100.9	99.5	98.5	98.2	100.4	100.0	100.3	99.8	99.1	99.6	100.9	101.0
Fo%	83.0	83.3	77.6	73.2	79.6	74.3	77.0	71.5	69.8	78.8	71.7	66.5	86.4	74.1	78.3	75.4	74.9	70.3	69.6	70.3
Fa%	17.0	16.7	22.4	26.8	20.4	25.7	23.0	28.5	30.2	21.2	28.3	33.5	13.6	25.9	21.7	24.6	25.1	29.7	30.4	29.7

(*continued on next page*)

Table 1 (*continued*)

	Post-caldera																			
	1787–1832			*1991*						*1995–2000*										
	BAR 1			BAR 25			BAR 6			BAR 16			BAR 10	BAR 11			BAR 14		BAR 12	
	Ph core	Ph rim	Mph core	Ph core	Mph core	Gdm	Ph core	Ph rim	Gdm	Mph core	Mph rim		Ph core	Ph core	Ph rim	Gdm	Mph core	Mph rim	Ph core	Ph rim	Gdm
SiO_2	38.3	37.2	37.3	40.2	39.8	39.4	38.5	37.5	36.2	38.2	37.8		38.4	38.9	39.2	41.0	38.9	37.7	38.5	38.3	38.3
FeO_{tot}	22.5	27.7	28.3	14.0	14.4	22.5	19.9	24.1	32.1	25.0	26.7		24.1	21.4	22.9	28.3	21.8	28.7	18.1	23.5	27.8
MnO	0.42	0.44	0.47	0.23	0.25	0.44	0.38	0.56	0.61	0.46	0.55		0.5	0.37	0.48	0.59	0.35	0.49	0.28	0.44	0.57
MgO	39.8	35.9	34.6	43.5	43.8	36.9	42.1	37.8	31.5	38.3	36.3		38.5	40.4	39.3	31.5	40.5	34.9	41.9	37.8	34.1
CaO	0.17	0.17	0.18	0.15	0.19	0.42	0.17	0.16	0.34	0.17	0.16		0.17	0.18	0.21	0.29	0.21	0.19	0.22	0.18	0.27
Cr_2O_3	0.03	0.07	–	–	–	–	0.04	–	–	–	–		–	–	–	–	–	–	–	–	0.01
Total	101.2	101.5	100.9	98.1	98.4	99.7	101.1	100.2	100.7	102.1	101.6		101.7	101.2	102.0	101.6	101.8	101.9	99.0	100.2	101.0
Fo%	75.9	69.8	68.5	84.7	84.4	74.5	79.0	73.6	63.7	73.2	70.7		74.0	77.1	75.8	65.7	76.8	68.4	80.5	74.2	68.6
Fa%	24.1	30.2	31.5	15.3	15.6	25.5	21.0	26.4	36.3	26.8	29.3		26.0	22.9	24.2	34.3	23.2	31.6	19.5	25.8	31.4

LPh, large phenocryst; Ph, phenocryst; Mph, microphenocryst; Gdm, groundmass.

2000 eruptions. All of them moved westward from lateral spatter cones and reached the shoreline where the caldera depression is open to the sea. Pyroclastics related to historic activities are almost entirely represented by loose fine to coarse ash and ballistics. Most of them were produced during the final phase of the 1991 eruption and, to some extend, during the 1995 eruption. They are composed by massive-to-parallel laminated thick bed of coarse ash completely covering the present caldera floor and the rim along its north-eastern sector. The 2000 event was possibly entirely effusive producing a small lava flow moving to the sea from the westward lateral crater. The 1995 and 2000(?) lava flows are still cooling as testified by a diffuse steaming from the ground surface. During the 2003 fieldwork the activity in the island was represented only by fumarolic emissions, at boiling point, from the inner flank of the summit craters and diffuse steaming from the external southwestern flank. It is worth to note that in 2008 the Indian Coast Guards have reported a profuse fumarolic activity from the central tuff cone. A few months after the 2004 tsunami and Sumatra earthquake, BI violently rejuvenated. The eruptive activity started in middle of May 2005 and lasted for almost two years. The volcanic events were repeatedly characterized by strombolian to vulcanian explosive episodes, accompanied by coarse to fine ash fall and followed by the emission of highly fragmented lavas. Pyroclastic materials were emitted from the central vent as well as from a newly formed vent located in the upper sector of the southern slope. Products of the 2005 activity has completely covered all the older pyroclastic deposits and lava flows The 2005 juvenile material is similar to those emitted during the 1994–95 eruptive activity, both being highly scoriaceous.

5. Results

During the fieldwork, rock samples, representative of different volcanic units (Fig. 5), and a fumarolic gas discharging from the inner part of the southernmost crater, were collected. The volcanic products consist of lavas, which represent by far the most common products of the island, dyke and pyroclastic deposits. Mineral chemistry, whole rock (major, trace elements and Sr and Nd isotope) compositions for the studied volcanic products are reported in Tables 1–3. Analytical procedures for both rock and gas samples are described in the Appendix. The complete data set of mineral phase composition is available on request from the authors.

Based on K_2O vs. SiO_2 (wt%) relationships (Peccerillo and Taylor, 1976), BI rocks display a restricted compositional range, varying from low-K tholeiitic basalts to low-K basaltic andesites (Fig. 9). It is worthwhile to mention that the prehistoric (precalderic) rocks, whose age has not been determined by radiometric methods, although attributed to the Neogene(?)/Late Pleistocene(?) (Ravi Shankar et al., 2001), are in the same compositional range of the recently emitted lava flows. The 1991 volcanic rocks have a more evolved composition with SiO_2 and K_2O concentrations varying from 53.8% to 56% (by wt.) and 0.5% to 0.7% (by wt.), respectively. Magmatic evolution of the BI rocks appears to be not continuous with time, as evidenced by the SiO_2 and Mg# vs. time diagram of Fig. 10. After the emission of magmas, of mainly basaltic composition (prehistoric and 1787–1832? AD), lavas erupted during the volcanic activity of 1991 were basaltic andesites. Successively, the basaltic magmas, similar in composition to those erupted in 1787–1832(?) were emplaced in 1995 and 2000(?). Major element analysis (Table 2) of a 2005 lava rock sample, collected west of the active cone at the base of the inner caldera wall, indicates a composition near the boundary between basalt and low-K tholeiite (Fig. 9).

Table 2
Major (wt %) and trace (ppm) element composition of the Barren rocks.

	Pre-caldera									
	BAR 24 lava flow	BAR 13 lava flow	BAR 18 lava flow	BAR 20 lava flow	BAR 21 lava flow	BAR 19 lava flow	BAR 5 lava flow	BAR 3 dyke	BAR 4 dyke	BAR 23 Lithic
SiO_2	49.8	50.5	50.8	50.8	51.9	52.2	53.5	48.8	49.6	55.8
TiO_2	0.74	0.70	0.65	0.80	0.86	0.83	0.68	0.74	0.75	0.85
Al_2O_3	15.7	18.6	18.3	20.8	18.2	20.6	17.6	16.7	16.7	17.6
FeOtot	8.4	7.5	7.3	7.1	7.5	6.8	7.0	7.8	7.9	7.5
MnO	0.17	0.15	0.16	0.15	0.16	0.14	0.15	0.15	0.15	0.17
MgO	11.4	7.7	7.8	4.7	7.1	4.7	6.7	10.9	11.0	4.9
CaO	10.7	11.3	10.6	11.0	10.0	10.3	9.8	10.7	10.9	8.4
Na_2O	2.3	2.4	2.7	2.9	3.1	3.3	3.2	2.3	2.4	3.8
K_2O	0.24	0.26	0.32	0.37	0.42	0.51	0.46	0.27	0.31	0.52
P_2O_5	0.06	0.07	0.08	0.11	0.11	0.14	0.11	0.08	0.08	0.13
L.O.I.	–	–	–	–	–	–	0.01	–	–	–
Mg#	70.9	64.6	65.6	54.0	62.7	55.0	62.9	71.3	71.4	54.0
Rb	4	6	5	7	7	11	9	6	5	10
Sr	151	177	186	244	222	250	199	203	204	188
Y	21	21	20	22	25	24	24	20	20	28
Zr	49	49	55	62	68	77	72	51	50	88
Nb	0.58	0.43	0.53	1.26	0.74	2.08	0.84	0.74	0.63	0.84
Ba	47	61	77	78	91	107	98	71	66	110
Ni	218	100	94	49	97	42	76	218	216	43
Cr	557	241	249	86	204	81	216	496	508	103
V	262	253	201	250	288	220	216	257	263	249
Sc	39	36	29	30	33	28	33	34	35	29

	Post-caldera														
	1787–1832			*1991*					*1995–2000*						*2005*
	BAR 1 lava block	BAR 17 lava flow	BAR 22 lava flow	BAR 25 scoria	BAR 6 lava bomb	BAR 16 lava flow	BAR 8 lava bomb	BAR 26 lava flow	BAR 2 lava flow	BAR 10 lava flow	BAR 11 lava flow	BAR 14 lava flow	BAR 15 lava flow	BAR 12 lava flow	BAR 9 lithic	BAR 28 lava flow
SiO_2	50.7	51.1	51.4	53.6	54.6	54.7	55.4	56.0	50.4	50.6	50.7	50.9	50.9	51.3	56.1	49.4
TiO_2	0.81	0.81	0.82	1.18	1.12	1.18	1.20	1.18	0.80	0.80	0.80	0.81	0.82	0.81	0.84	0.86
Al_2O_3	21.2	21.3	21.3	18.0	18.2	17.6	17.4	17.5	21.0	21.1	21.0	21.3	21.4	21.4	19.1	21.2
FeOtot	6.9	6.9	7.0	8.8	8.3	8.6	8.6	8.4	6.8	6.9	6.9	6.9	6.9	6.9	3.0	8.4
MnO	0.14	0.15	0.15	0.18	0.18	0.19	0.19	0.19	0.14	0.15	0.14	0.14	0.15	0.14	0.02	0.14
MgO	3.8	3.9	4.0	4.0	3.9	3.6	3.7	3.5	3.8	4.1	4.0	3.9	3.9	3.8	5.3	4.3
CaO	11.3	11.3	11.3	9.2	8.8	8.2	8.1	7.8	11.1	11.3	11.2	11.3	11.3	11.2	9.8	11.0
Na_2O	2.9	3.0	3.0	3.5	3.9	4.1	4.1	4.3	2.9	3.0	2.9	2.9	2.9	2.9	4.6	3.5
K_2O	0.39	0.39	0.39	0.51	0.62	0.65	0.68	0.69	0.40	0.38	0.39	0.38	0.39	0.39	0.27	0.40
P_2O_5	0.10	0.10	0.10	0.13	0.15	0.16	0.17	0.17	0.10	0.10	0.10	0.09	0.09	0.10	0.10	0.10
L.O.I.	–	–	–	0.06	–	–	–	–	–	–	–	–	–	–	–	0.14
Mg #	49.5	50.0	50.3	44.7	45.6	42.8	43.0	42.3	49.8	51.0	50.7	50.2	50.2	49.7	75.8	47.8
Rb	10	10	10	12	17	18	19	19	10	10	10	10	10	10	3	n.d.
Sr	219	216	217	190	202	195	204	194	219	217	216	217	216	216	215	n.d.
Y	24	23	24	32	34	36	37	38	24	23	23	23	23	23	25	n.d.
Zr	62	61	63	84	94	101	103	107	63	61	62	62	61	61	59	n.d.
Nb	0.63	0.63	0.63	0.74	1.46	0.74	1.57	1.05	0.74	0.63	0.74	0.53	0.53	0.53	0.63	n.d.
Ba	86	80	84	99	121	128	144	137	84	84	86	77	80	83	70	n.d.
Ni	26	22	24	21	21	10	16	9	27	25	28	24	21	24	50	n.d.
Cr	43	36	43	36	32	14	14	10	43	47	45	41	40	42	171	n.d.
V	277	285	264	429	347	349	371	327	292	270	286	290	283	295	256	n.d.
Sc	29	29	28	40	34	35	35	31	29	28	29	30	29	29	31	n.d.

n.d. = not determined.

5.1. Petrography and mineral chemistry

The BI volcanic products have been divided into two groups: (1) the pre-caldera rocks and the associated dyke, and (2) the post-caldera rocks, including the 1787–1832(?), 1991 and 1995–2000(?) events. No mineral chemistry data on the 2005 lava are presently available.

5.1.1. Pre-caldera products

They consist of porphyritic basaltic and basaltic andesitic lava flows (Fig. 9) with a phenocryst content varying from 30% to 45% by volume. Plagioclase (plg) is often the most abundant mineral phase with subordinate contents of olivine (ol) and clinopyroxene (cpx), although a few samples (e.g. BAR 3 and 18) are very rich in olivine and clinopyroxene. An interesting feature of these rocks is the presence of large phenocrysts (>2 mm) of plg, ol and cpx in variable concentrations. However, while large phenocrysts of plg are ubiquitous, those of ol and cpx are more sporadic. A xenocrystic origin has been hypothesized for these crystals (Luhr and Haldar, 2006). Fe–Ti oxides occur as accessory mineral phases. Groundmass is relatively heterogeneous and represented by holocrystalline intergranular to intersertal fluidal to aphanitic textures. In the groundmass microlites representative of the main mineralogical assemblage have been recognized. Dyke intruding the pre-cal-

Table 3
Trace element (ppm) and Sr and Nd isotope composition of selected Barren volcanics.

	Pre-caldera					Lithic	Post-caldera					Lithic
	BAR 24	BAR 13	BAR 19	BAR 5	BAR 3	BAR 23	BAR 1 *1787–1832*	BAR 25 1991	BAR 16	BAR 11 1995–2000	BAR 14	BAR 9
Cs	0.16	0.24	0.39	0.2	0.36	0.14	0.37	0.54	0.66	0.41	0.39	0.15
La	2.40	2.83	6.70	5.00	4.40	5.00	4.64	5.80	7.90	4.76	4.55	3.06
Ce	6.80	7.50	16.00	12.70	11.03	13.10	11.78	15.20	20.09	11.98	11.65	8.20
Pr	1.14	1.17	2.28	1.88	1.69	2.00	1.82	2.26	2.98	1.80	1.78	1.26
Nd	6.11	6.10	10.70	9.10	8.20	9.90	8.87	11.70	14.21	8.76	8.54	7.10
Sm	2.10	2.01	3.10	2.58	2.33	2.94	2.57	3.59	4.06	2.68	2.55	2.52
Eu	0.84	1.02	1.28	0.92	0.81	1.08	0.97	1.32	1.39	0.89	0.99	0.84
Gd	2.59	2.64	3.09	3.20	2.67	3.61	3.07	3.90	4.65	3.01	2.98	3.05
Tb	0.49	0.47	0.55	0.57	0.48	0.66	0.57	0.72	0.84	0.54	0.56	0.54
Dy	3.29	2.88	3.80	3.50	3.19	4.10	3.71	4.80	5.56	3.69	3.71	3.90
Ho	0.72	0.66	0.78	0.79	0.69	0.94	0.80	1.08	1.24	0.80	0.81	0.88
Er	2.12	1.89	2.24	2.33	1.97	2.77	2.28	3.03	3.44	2.29	2.32	2.36
Tm	0.33	0.30	0.36	0.38	0.29	0.46	0.36	0.50	0.55	0.36	0.37	0.35
Yb	2.01	1.78	2.23	2.33	1.91	2.62	2.25	3.10	3.43	2.20	2.25	2.43
Lu	0.31	0.26	0.33	0.35	0.28	0.41	0.33	0.44	0.50	0.33	0.33	0.34
Hf	1.33	1.40	1.86	1.93	1.36	2.30	1.66	2.08	2.60	1.62	1.69	1.62
Ta	0.047	0.051	0.12	0.067	0.052	0.071	0.050	0.067	0.076	0.058	0.047	0.084
Pb	0.86	2.21	2.44	1.76	1.30	1.55	1.58	2.81	2.56	1.60	1.48	1.00
Th	0.39	0.58	1.58	1.10	0.89	1.08	1.30	1.32	2.42	1.28	1.28	0.56
U	0.093	0.11	0.25	0.23	0.15	0.24	0.21	0.24	0.40	0.22	0.20	0.12
$(La/Sm)_n$	0.71	0.88	1.34	1.21	1.18	1.06	1.13	1.00	1.22	1.11	1.11	0.76
$(La/Yb)_{*n}$	0.81	1.08	2.03	1.46	1.56	1.30	1.40	1.26	1.57	1.47	1.38	0.85
Eu/Eu	1.10	1.35	1.27	0.98	0.99	1.02	1.06	1.08	0.98	0.96	1.10	0.92
$^{87}Sr/^{86}Sr$	0.703805	0.703891	0.704000	0.703982	0.703903	0.703878	0.703995	0.704008	0.704030	0.704001	0.704000	0.704130
$^{143}Nd/^{144}Nd$	0.513005	0.512952	0.512904	0.512927	0.512929	0.512967	0.512887	0.512926	0.512860	0.512864	0.512890	0.512973

dera lavas (BAR 3, BAR 4) has a basaltic composition and shows hypocrystalline highly porphyritic texture (Alam et al., 2004). Plagioclase microlites in the groundmass are at places isoriented. Among the phenocrysts, femic minerals (cpx and ol) are more abundant than those of plg. Large phenocrysts of plg, cpx and ol are also observed. Lithic samples (e.g. BAR 23) collected in a pericalderic pyroclastic deposit display holocrystalline texture and a relatively high phenocryst content. Plagioclase is the dominant mineral and occurs both as phenocryst and microphenocryst; minor cpx, rare ol and small Fe–Ti oxides are also observed.

5.1.2. Post-caldera products

1787–1832(?) rocks: they are basaltic in composition and highly porphyritic (40–50% by vol.); the texture is holocrystalline or hypocrystalline seriate. Phenocrysts mainly consist of plg, whereas cpx and ol are subordinated. This mineral assemblage along with Fe–Ti oxides also dominates the groundmass; large phenocrysts of plg are ubiquitous.

1991 rocks: the volcanic products from 1991 eruption have a basaltic andesitic composition. They consist of lavas, scoriae and bombs displaying vacuolar, glassy texture; phenocrysts are present from 10% to 15% by vol. and consist of plg with lower amount of ol and cpx set in a hyalopilitic, fluidal groundmass. Plagioclase rarely occurs as microlite in the groundmass. Fe–Ti oxides are rare.

Hypo-abyssal lithic samples (e.g. BAR 9) show a gabbroic composition and are characterized by a porphyritic texture with zoned plg and rare cpx phenocrysts. The groundmass is composed by plg, cpx and abundant Ti-magnetite and ilmenite.

1995–2000(?) rocks: the composition of these products is basaltic. Texture is generally hypocrystalline or holocrystalline with a relatively high porphyritic index (30–40%). Plagioclase and subordinate cpx and ol phenocrysts are set in a microcrystalline groundmass containing the same mineral phases. Large phenocrysts of plagioclase are ubiquitous. Opaque minerals are mainly represented by Ti-magnetite and ilmenite.

2005 rocks: the studied lava samples display petrographic characteristics similar to those of the 1995–2000(?) products. In these

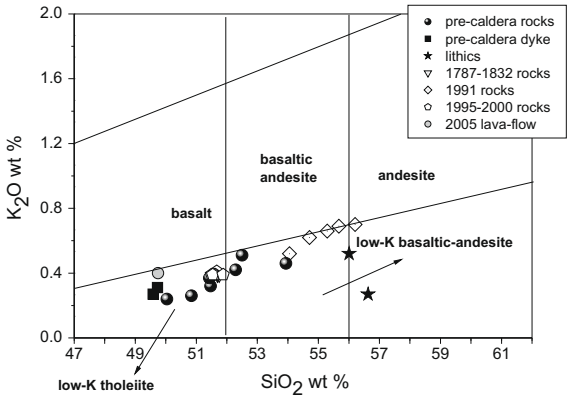

Fig. 9. K_2O vs. SiO_2 (wt%) classification diagram (Peccerillo and Taylor, 1976). Chemical data are plotted on water-free basis.

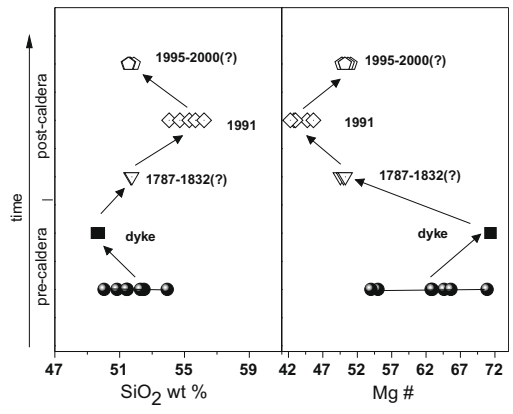

Fig. 10. SiO_2 and Mg# variation with time in the Barren volcanics. Symbols as in Fig. 9.

lavas, in addition to plagioclase, large phenocrysts of clinopyroxene are also abundant.

Independently from the different eruptive cycles, no significant difference among the petrographic features and the mineral chemistry of the studied rocks, has been observed. Here below the salient characteristics of the main mineralogical phases are reported.

Plagioclase: generally consists of euhedral or subhedral crystals, variously twinned, often displaying sieve texture or patchy zoning. Zoning is slight, generally normal and only in few cases is reverse (e.g. BAR 19). Rims display in some crystals oscillatory zoning and inclusions of glass and/or Fe–Ti oxides. Plagioclase phenocrysts and large phenocrysts, up to 5 mm in diameter, have a highly Ca-rich core (An = 80–95% and 90–95%, respectively). They often display an abrupt compositional variation between core and rim, marked by a dissolution surface. A similar anorthitic compositional range is found in the hypo-abyssal lithic samples. Large phenocrysts shows An compositional variability in the range 45–85%. Microphenocryst cores display sometimes an anorthitic content higher than that of the coexisting phenocrysts. Microlites have an anorthitic content between 44% and 70%, partly overlapping those of the microphenocrysts and phenocryst rims. Ca-rich plg crystals have widely been documented in basic-intermediate volcanic rocks from subduction zone around the world (e.g. Yoder, 1969; Dungan and Rhodes, 1978; Marsh et al., 1990). Their crystallization is considered the effect of high water content in the melt shifting plagioclase to high calcic composition (e.g. Sisson and Grove, 1993; Kohut and Nielsen, 2003).

Pyroxene is colorless, euhedral to rounded, dusty and frittered. Large (up to 4 mm) and abundant crystals are only referred to the pre-caldera rocks. Zoning is slight, generally normal or rarely reverse. Clinopyroxene is prevalently augitic and diopsidic; phenocryst core compositions are in the range Wollastonite 42–47%, Enstatite 42–46%, Ferrosilite 7–16% with Mg# 60–87. Pigeonite sometimes occurs in the groundmass, whereas clinoenstatite is found as phenocryst in a pre-caldera rock sample (BAR 19) and in the hypo-abissal lithic samples (e.g. BAR 9). Notably, in the latter, augite and clinoenstatite phenocrysts coexist. Finally, in few cases pigeonite and clinoenstatite constitute olivine rims. Rare microphenocrysts, showing higher Mg# than that of the coexisting phenocrysts, occur.

Olivine is present as colorless anhedral and/or corroded crystals. Large phenocrysts (only in the pre-caldera rocks) are up to 3.5 mm in size. Olivine exhibits skeletal or parallel-growth crystals. Some (particularly from the pre-caldera period) olivines are partially transformed to iddingsite or mantled by cpx and orthopyroxene. Chromite is often included in the olivine crystals. Olivine core composition is in the range Forsterite (Fo) 70–86%. Microphenocrysts and rim of phenocrysts are generally of composition Fo 70–60%. Zoning is normal and slight.

Glomerophyric aggregates of plagioclase, clinopyroxene, olivine and oxide are ubiquitous; the compositional variation of the mineral phases is similar to that observed for the pheno-and microphenocrysts.

As described, the compositional features of the mineral phases do not significantly change with time; notably, evidence of disequilibrium is often observable in all the different volcanic products.

5.2. Whole rock- and fluid-geochemistry

5.2.1. Major and trace elements

BI rocks are essentially composed of basalts and basaltic andesites and exhibit a content of Al_2O_3 typical of high-alumina basalts (e.g. Kuno, 1960; Crawford et al., 1987). They define a linear low-K trend in the alkali vs. SiO_2 diagram (Fig. 9), where only a few 1991 rocks cross the boundary between the low-K tholeiite and calc-alkaline fields. In terms of FeOtot/MgO versus SiO_2 (Fig. 11), all the post-caldera rocks fall in the tholeiitic field, whereas the pre-caldera rocks, with the exception of one rock sample (BAR 20), plot in the calc-alkaline area.

Major and trace element data are listed in Tables 2 and 3, whilst Harker's diagrams for some major and trace elements are shown in Figs. 12 and 13.

A few rock samples, particularly those from the pre-caldera phase, are slightly scattered, suggesting heterogeneous accumulation of mineral phases. Negative correlations between CaO and MgO versus SiO_2 are observable, whereas Na_2O, P_2O_5, and K_2O (Fig. 9) display an opposite behavior. In the Al_2O_3 vs. SiO_2 plot, where the lowest values correspond to the less evolved rocks, though the values of the pre-caldera rocks are scattered, it is possible to observe a typical Al_2O_3 trend. A weak positive correlation exists between TiO_2 and MnO (not shown) and SiO_2.

Among the trace elements, a positive correlation between LILE and HFSE versus SiO_2 is observed. Ferromagnesian elements, such Cr (not shown) and Ni display an overall decrease, exhibiting a curvilinear trend. Strontium shows scattered abundances, likely related to different abundance of plagioclase. Ratios of incompatible trace elements versus SiO_2 (Fig. 14), such as Ba/Nb and La/Nb, not modified from evolutionary processes, do not display significant correlations with SiO_2, being relatively scattered, and showing nearly similar values for both basaltic and basaltic andesitic rocks; Ba/Rb and Rb/Sr ratios versus SiO_2 define a roughly negative and positive correlation, respectively. As evidenced in most of the variation diagrams, the 1787–1832(?) and 1995–2000(?) rock samples display similar major and trace element abundances (e.g. Al_2O_3, MgO, Ni) and trace element ratios, forming a distinct group of samples. Chondrite-normalized (McDonough and Sun, 1995) La/Yb_n ratios vary from 0.81 to 2.03 (Table 3) and La/Sm_n shows an overall increase from basalts to basaltic andesites (Fig. 15). The pre-caldera rocks include both slightly LREE fractionated patterns with flat HREE, both light-REE depleted and flat HREE patterns. Few samples (e.g. BAR 13 and BAR 19) display a positive Eu anomaly (Eu/Eu^*: 0.92–1.35). Post-caldera rocks show patterns with very slight fractionation. The 1787–1832(?) and 1995–2000(?) rocks show identical patterns with two of them displaying also a slight positive Eu anomaly.

Mantle-normalized (Sun and McDonough, 1989) incompatible trace element patterns of BI basalts (Fig. 16) are typical of island–arc basic and intermediate rocks (e.g. Gill, 1981); they are characterized by a moderate fractionation, negative anomalies of Ta, Nb and Ti, positive spikes of K and Pb and slight enrichment of Sr in the pre-caldera rocks. Pre-and post-caldera products display an overall parallelism of the patterns with the pre-caldera

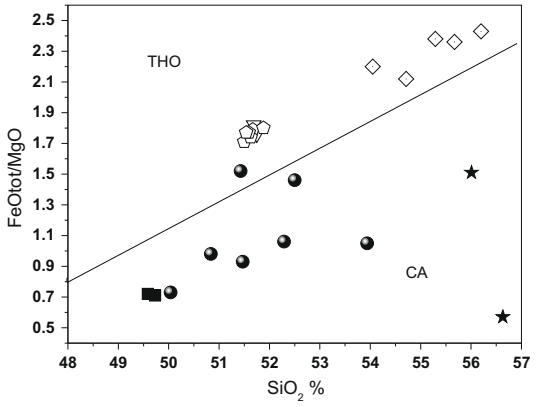

Fig. 11. FeOtot/MgO vs. SiO_2 binary diagram. TH: tholeiitic suite; CA: calc-alkaline suite. The straight line separates the two suites (from Wilson, 1989).

rocks showing a minor enrichment for the most incompatible elements. In particular, the pre-caldera BAR 24 sample represents the least enriched rock. In the Fig. 16, for comparison, the pattern corresponding to the mean composition of two lavas from Galunggung (Sunda Arc), considered primitive tholeiitic basalts (Turner and Foden, 2001), is also reported. The composition of these basalts fall for several elements in the range of the Barren pre-caldera rocks but are more enriched in Cs and depleted from Hf to Yb.

5.2.2. Sr and Nd isotopes

Sr isotopic ratios vary from 0.70380 to 0.70403 with the wider variability observed in the pre-caldera volcanic products; in particular, the pre-caldera BAR 24 rock displays the lowest $^{87}Sr/^{86}Sr$ ratio whereas the highest values are associated with the more evolved rocks (Fig. 17); the $^{87}Sr/^{86}Sr$ ratio (0.70413) found in the hypabyssal lithic BAR 9 testifies the presence of magmas with high Sr isotopic ratios. The Nd isotope ratios are in the range 0.512860–0.513005 and display an overall negative correlation with $^{87}Sr/^{86}Sr$ (Fig. 17). The variation of the Sr isotopic ratios versus Ba, Sr, Rb and La abundances shows a positive correlation (Fig. 18). The scattered positive correlation defined by $^{87}Sr/^{86}Sr$ and Th/Ta ratios, which is considered to reflect slab contribution, and the negative correlation between Nd isotope ratios and Th/Ce ratios (Fig. 18) are consistent with the addition of sediments to the mantle source.

5.2.3. Fluid geochemistry

Several diffuse gas emissions (steaming grounds) were recognized in different areas of the intra-caldera nested craters. The difficulties in finding suitable spots where to sample crater fumarolic discharges have allowed the collection in February 2003 of only one gas sample for chemical and isotopic analysis from the emission site characterized by the highest flux and located in the southern rim of the central polygenic tuff cone. This sample was mainly composed of water vapor (931,321 μmol/mol), CO_2 (35,356 μmol/mol) and N_2 (15,113 μmol/mol), whereas highly acidic compounds, such as SO_2, HCl and HF, commonly found in medium-to-high fumaroles from active volcanic systems (Giggenbach, 1996), were below the detections limits (0.01 μmol/mol). As a consequence, at the time of sampling the chemical composition of the sampled fumarole had no clues of a direct contribution from a magmatic source. Even the high H_2 content (5752 μmol/mol), which could be related to high-temperature fluids, can be explained in terms of prevailing hydrothermal-type reducing conditions. Typical hydrothermal gas compounds, e.g. CH_4 and H_2S, have relatively high contents (338 and 45 μmol/mol, respectively), whereas CO, which in shallow aquifers easily hydrolyzes to produce formic acid (Shock, 1993), was not detected. In contrast, the isotopic ratios of both helium (R/Ra = 5.1) and carbon (δ^{13} C–CO_2 = −2.94‰ PDB) have a clear mantle signature. Therefore, it can be deciphered that at BI a well-developed hydrothermal system seems to lie at rela-

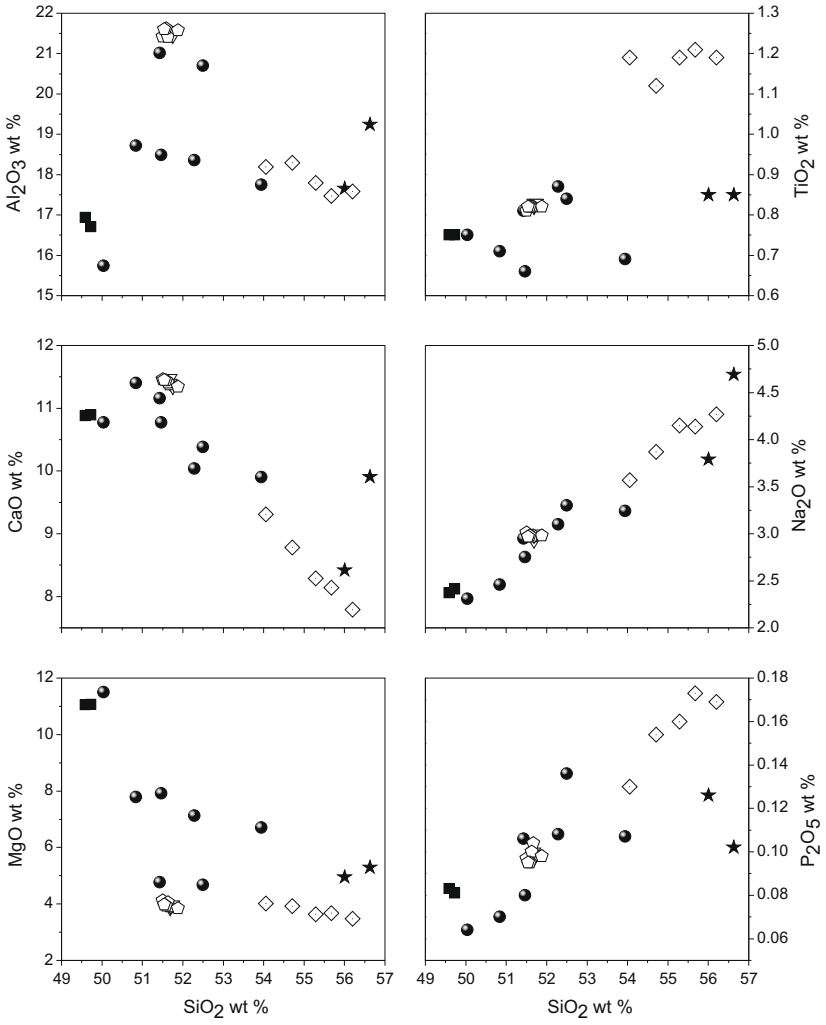

Fig. 12. Harker's diagrams for some major (wt.%) elements. Symbols as in Fig. 9.

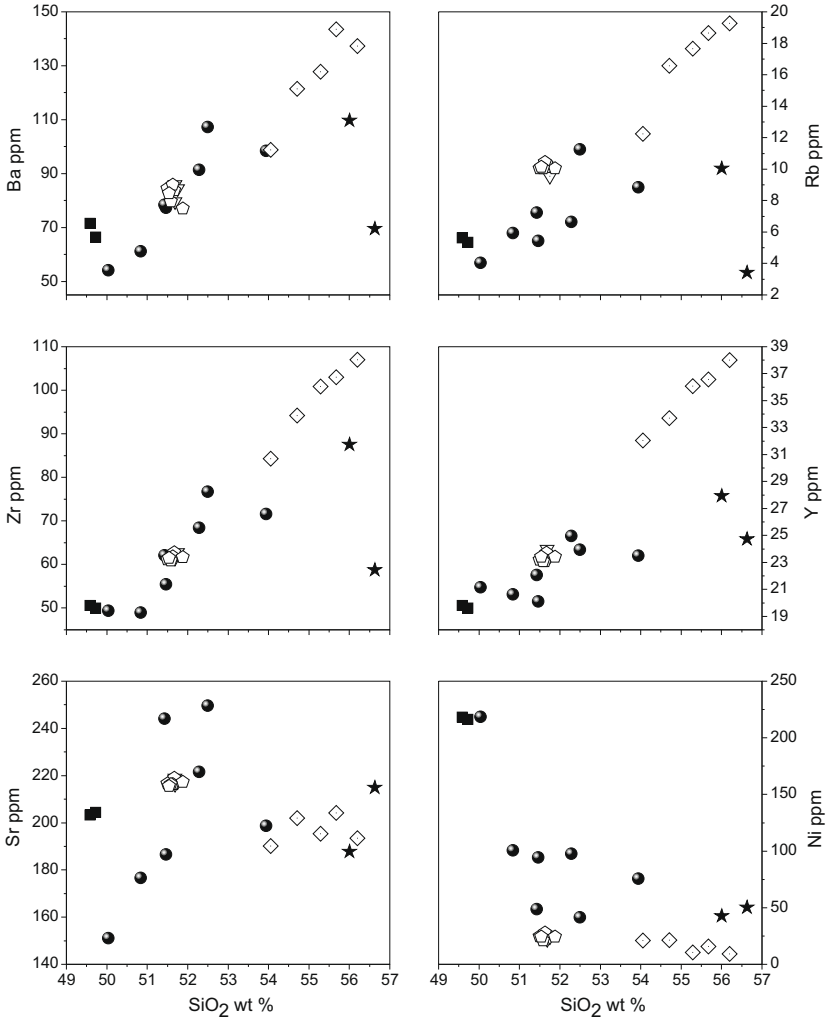

Fig. 13. Harker's diagrams for some trace elements (ppm). Symbols as in Fig. 9.

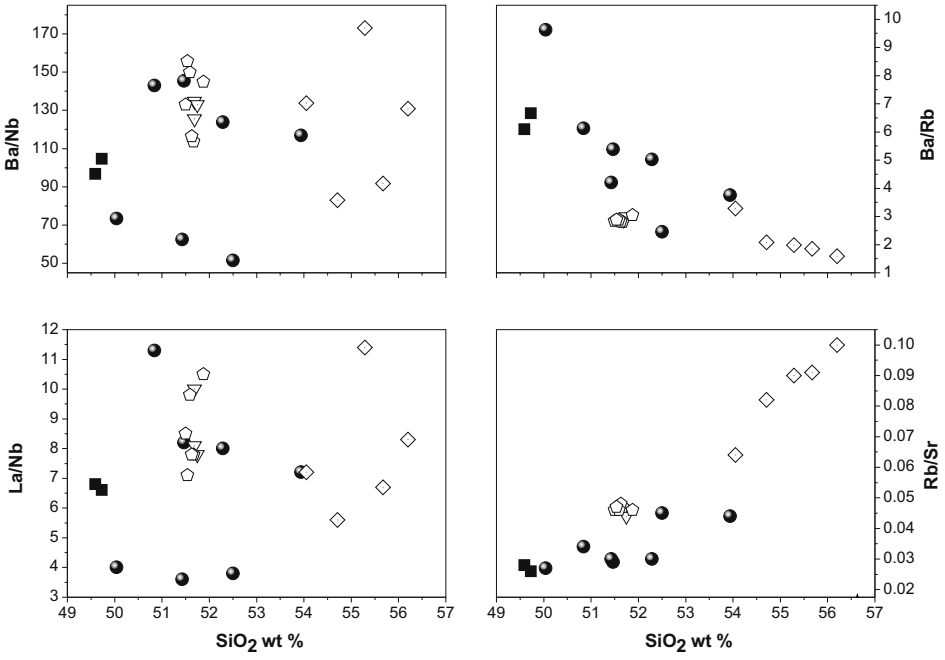

Fig. 14. Variation diagrams of incompatible element ratios versus silica. Symbols as in Fig. 9.

tively shallow depth, promoting secondary interactions capable of masking the presence of uprising magmatic gases and/or that no degassing magmas were stored at shallow depth. Geothermometric calculations based on the temperature dependence of both fH_2 (Giggenbach, 1991) and the CO_2–CH_4 pair under the control of the FeO–Fe_2O_3 redox buffer (rock buffer; Giggenbach, 1987) indicate an equilibrium temperature of about 300 °C. This seems to support the hypothesis that the chemical features of the discharged fluids were established at a certain depth within the hydrothermal reservoir. Accordingly, the 2005 eruptive activity could have been triggered by new inputs of fresh, undegassed magma at shallow depth.

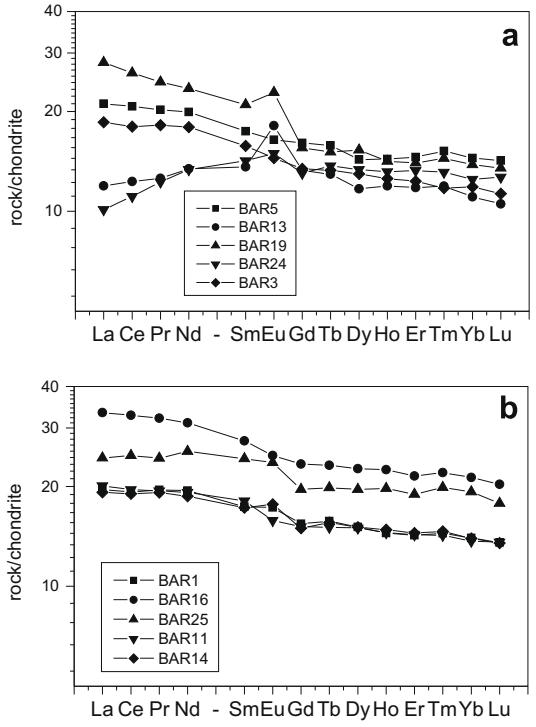

Fig. 15. Condrite-normalized (McDonough and Sun, 1995) REE patterns for the BI rocks. (a) pre-caldera rocks; (b) post-caldera rocks.

6. Discussion

The BI volcanic products show a relatively narrow compositional range: from low-K basalts to basaltic andesites. More evolved compositions (SiO_2 > 59%) are reported by Luhr and Haldar (2006) for two pre-caldera pumices. The lack of depositional records clearly related to caldera-forming eruption together with the absence of highly chemically evolved magmas, could suggest a lateral landslide as the most probable process responsible for the caldera formation. The BI volcanics form a single tholeiitic trend in the K_2O vs. SiO_2 diagram and the described common petrochemical characteristics suggest a comagmatic origin for all the magmas. Nevertheless, some differences in the volcanic products emplaced during the eruptive history of BI can be highlighted. The general trends observed in the variation diagrams of Figs. 12 and 13 indicate that a crystal–liquid fractionation process has played a major role in determining some of the petrologic and geochemical characteristics of the BI magmas. However, a more complex petrogenetic history has to be invoked considering: (a) the presence of large phenocrysts of possible xenocrystic origin, (b) the variability of the ratios between incompatible trace elements in the basaltic rocks (Fig. 14), (c) the significant variations of the Sr isotopic ratios (Fig. 17) and (d) the relationships between the $^{87}Sr/^{86}Sr$ ratios and trace elements (Fig. 18). These chemical and

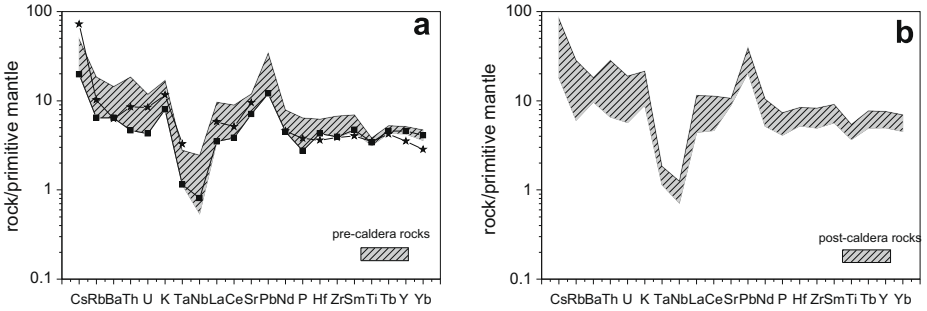

Fig. 16. Mantle-normalized (Sun and McDonough, 1989) incompatible trace element patterns for the BI rocks. (a) Range of pre-caldera rocks; squares correspond to BAR 24 rock sample, stars to the Galunggung (Sunda Arc) primitive tholeiitic basalt (Nb and Pb lacking; data from Turner and Foden, 2001); (b) range of post-caldera rocks.

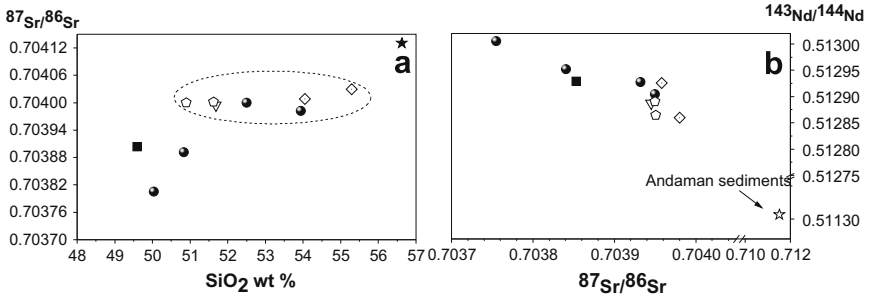

Fig. 17. Variation diagrams of Sr isotope ratios versus SiO_2 and $^{143}Nd/^{144}Nd$ vs. $^{87}Sr/^{86}Sr$. (a) The dotted ellipse indicates rock samples with similar $^{87}Sr/^{86}Sr$; (b) open star represents the estimated bulk composition of sediments subducting beneath the Andaman arc (Plank and Langmuir, 1998). Symbols as in Fig. 9. See text for details.

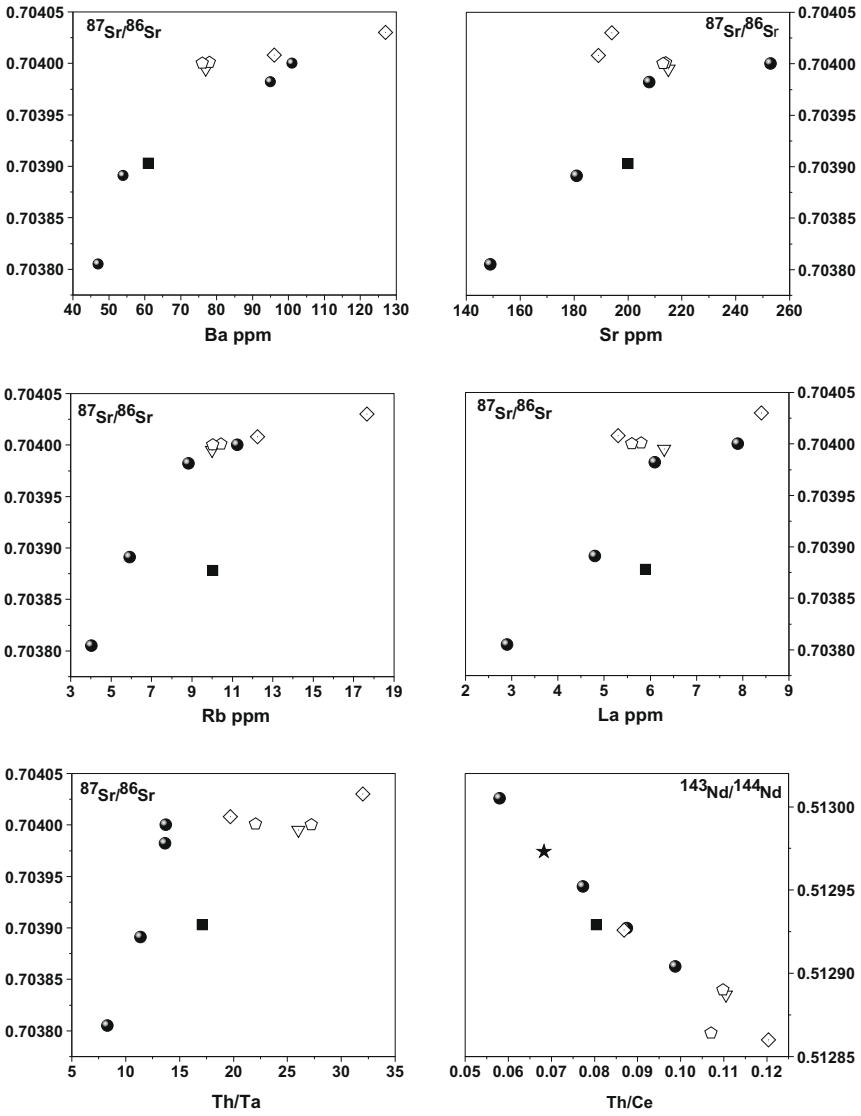

Fig. 18. Variation diagrams of Sr isotope ratios versus Ba, Sr, Rb and La concentrations and Sr isotope ratios versus Th/Ta ratios and Nd isotope ratios versus Th/Ce ratios. Symbols as in Fig. 9.

isotopic features point to the occurrence of additional evolutionary processes and/or to a role likely played by a heterogeneous magma source. The formation of the caldera represents an important episode in the history of BI, and the pre-and post-caldera magmas likely reflect a modification of the magmatic plumbing system. Pre-caldera magmas show a general less evolved composition (i.e. high Mg# and Ni and Cr contents, Table 2), a distinctively scattering behavior of major and trace elements (Fig. 12) and a certain variability in terms of Sr and Nd isotopic ratios (Figs. 17 and 18). On the contrary, post-caldera magmas have a more homogeneous composition with relatively constant $^{87}Sr/^{86}Sr$ and $^{143}Nd/^{144}Nd$ isotopic ratios that correspond to the highest and lowest, respectively, values measured in the studied volcanic products.

6.1. Pre-caldera magmas

Most of the Barren magmas are low-K tholeiites (Fig. 9) and the pre-caldera products display the lowest degree of evolution. In the Sunda Arc, other tholeiitic rocks have been found at Galunggung; they are considered near-primitive lavas (MgO = 10.6–12.5%; Turner and Foden, 2001) representing the best estimated composition of unmodified mantle melt entering the crust (Gerbe et al., 1992). The trace element pattern corresponding to the mean Galunggung tholeiitic basalts (Fig. 16) shows higher abundances of the most incompatible trace elements, except Ba, and almost similar or lower abundances of Nd to Yb elements when compared to BAR 24 (Tables 2 and 3). For the Sunda low-K tholeiite lavas, Stolz et al. (1990) suggested a derivation from a MORB-type source, enriched by fluids and sediments from the subducting plate. An estimation of the Sr and Nd isotopic composition of the sediments subducting beneath the Andaman arc has been made by Plank and Langmuir (1998) and is shown in Fig. 17. The possible contribution of different components in the source of Sunda low-K tholeiites has been evaluated by Turner and Foden (2001) by using the Sr and Nd isotopic ratios and the ratios of immobile elements, such as Th/Ce and U/Th. These data indicate that fluids derived from an altered oceanic crust and a sediment component may have been added as a partial melt. Most of BI pre-caldera magmas have low $^{87}Sr/^{86}Sr$ and high $^{143}Nd/^{144}Nd$, low Pb isotope values (data from Luhr and Haldar, 2006) and low Th/Ce and U/Th ratios. This would imply little or no contribution from fluids and/or sediments in the source. We hypothesize, for the mantle source of BI magmas, an end member as that inferred from Turner and Foden (2001), i.e. the Indian Mid-Ocean Ridge Basalt (I-MORB). This can be particularly true

for the most primitive BI magma (BAR 24: Mg# = 71, Ni = 218 ppm, Cr = 557 ppm), displaying the lowest Th (0.39 ppm) content in the arc and, thus, representing an important reference composition in the Indonesian Arc study.

Moreover, as previously mentioned, the BI pre-caldera magmas display a heterogeneous composition and a small but significant variation of the Sr isotopic ratios. Unfortunately, no information about the time of emplacement of these rocks and the different eruptive phases is available. Generally speaking, the isotopic variability in magmas erupted by a single volcano could reflect either source heterogeneities or to be the effect of evolutionary processes. However, magmas obtained by melting of a heterogeneous source generally show increase of incompatible trace element abundances with increasing Sr isotopic signatures. The pre-caldera Barren magmas show scattered incompatible trace element ratios, such as Ba/Nb and La/Nb (Fig. 13), which do not correlate with any evolutionary parameter. This peculiarity is observed also for the post-caldera basic magmas, which display almost similar range of Ba/Nb and La/Nb values in the basaltic andesites. This fact could indicate that they are independent of evolutionary processes and that several characteristics of the basaltic Barren magmas have been inherited from the source.

6.2. Post-caldera magmas

The post-caldera magmas display almost constant and relatively high $^{87}Sr/^{86}Sr$ isotopic ratios (clustering around 0.7040), similar to the highest values found in the pre-caldera rocks. Some petrologic and geochemical characteristics observed among the post-caldera magmas are in agreement with the hypothesis that a FC process was able to drive the magma composition from basaltic to basaltic andesitic. In principle, this evolutionary process can quantitatively be tested for major (Stormer and Nicholls, 1978) and trace elements using different starting magma compositions, both pre-caldera (such as BAR 19) and post-caldera (such as BAR 1, from the 1787 eruptive phase) basaltic rocks displaying similar Sr isotopic ratio. However, the BI basaltic rocks are characterized by the ubiquitous presence of anorthite-rich (An > 90%) large plagioclase phenocrysts and, less frequently, large phenocrysts of olivine and clinopyroxene. Recently, Luhr and Haldar (2006) interpreted the Barren anorthitic plagioclase, and, possibly, the associated Mg-rich olivine and clinopyroxene crystals, as the product of desegregation of troctolitic crystal mushes or plutonic xenoliths. According to these authors, they have a xenocrystic origin. As they entered the magma, the bulk composition was modified to lower SiO_2 and higher Al_2O_3 contents. We evaluated the composition of mineral phases in equilibrium with the BI basaltic magmas by means of the on-line Java-based MELTS program (Ghiorso and Sack, 1995; Asimov and Ghiorso, 1998); on performing MELTS thermodynamic simulations at variable P_{tot} and H_2O%, we found that the composition of BI Ca-rich plagioclase is in disequilibrium with the whole rock composition. In agreement with the MELTS results is the presence of similar Ca-rich plagioclase in all Barren rocks and in the intrusive lithic (e.g. BAR 9), despite the fact that the latter display different silica content, testifying the xenocrystic origin of the plagioclase. On the contrary, olivine and clinopyroxene crystals, independently by their size, show a composition that could be in equilibrium with the host rock. As a consequence, in order to perform quantitative model, taking into account the high content of plagioclase xenocrysts, we recalculated the starting magma composition subtracting 10–15% of plg (assumed as the % of plg of xenocrystic origin). The simulation indicates that a variable solid fractionation of about 25–30% is able to reproduce the observed major element trends. The fractionating mineral assemblage is dominated by plagioclase (about 20%), with minor clinopyroxene (about 3–5%), olivine (3–1.5%) and Ti-magnetite as accessory mineral. However, some problems are encountered with the trace elements when trying to model the FC process by the Rayleigh fractionation equation. This mechanism cannot indeed generate the abundances observed for all trace elements: Rubidium and Barium are usually more enriched in the BI rocks than in the calculated model whereas Ni and Cr are less enriched. This characteristic can partly be imputed to the uncertainties of the quantitative model but it also suggests the occurrence of another evolutionary process that superimposed its effects on those determined by the crystal–liquid fractionation. Such a mechanism could be a mixing process between batches of magmas having different evolutionary degree. Mixing processes between more evolved magmas and basic liquids are also supported by the disequilibrium evidence furnished by the mineral chemistry data and finally, by the return to more basic compositions observed during the volcanological history of BI volcano.

6.3. Hydrothermal versus magmatic gases

The relatively low temperature discharges from the fumarolic vents (<100 °C) and the dominance of a H_2O–CO_2 gas mixture with significant contents of atmospheric gases, suggest a typical phenomenon of passive degassing from open volcanic systems. The carbon and helium isotopic ratios are typically mantle-related, although the relatively low R/Ra value (5.1) with respect to that expected for a MORB (ca. 8) highlights a dilution with a shallow hydrothermal system or mixing processes with a crustal component. It can be speculated about the low outlet temperatures and the lack of a clear magmatic signatures of the fumarolic discharges.. This can be due to both low magmatic fluid pressure, not able to be built up after the various eruptive events, and the high permeability of the system that facilitates a rapid permeation of the fluids throughout the central polygenetic tuff cone jeopardizing the formation of the typical fumarolic vents and/ or the lack of a still degassing magma at depth. These may be also favored by the selective removal (scrubbing; Symonds et al., 2001) of the most acidic gases (e.g. SO_2, HCl and HF) thanks to the interaction with deep saline and shallow fresh waters.

7. Concluding remarks

After the great December 2004 Sumatra earthquake and tsunami that has killed hundreds of thousands of people, the volcanic activity at Barren Island resumed in May 2005. This likely indicates the tight link between tectonics and magmatism in a complex system such as that of the Burma–Andaman–Java subduction area. Furthermore, Barren Island has awoken in 1991 after almost 140 years of a dormant phase. In these last 17 years the frequency of volcanic activity of the island is apparently increasing. As a consequence, the geochemical investigation and the depositional features of the emitted volcanic products and the chemical and isotopic features of the fumarolic discharges are important to both reconstruct the past activity and provide inferences on the future evolutive changes. Nevertheless, Barren Island consists of a caldera, possible related to a giant, lateral landslide of the original cone instead of a vertical collapse of a surficial magma chamber. The transition from pre-(less evolved) to post-caldera (slightly more differentiated) products is marked by the presence of hydromagmatic deposits, which have been described for the first time in this study.

Some interesting petrogenetic aspects have derived when considering sample BAR 24 that is characterized by high Mg# (71) value and Ni (218 ppm) and Cr (557 ppm) contents and displays the lowest Th (0.39 ppm) content in the whole arc. This finding represents an important reference composition for the Burma–Andaman–Java Arc.

Acknowledgements

The field trip of DC, BC, PM and OV was partly supported by a CNR bilateral project (Resp. O. Vaselli) and the Indian Institute of Technology.The Indian Coast Guard is warmly acknowledged for the logistic support and for the help of the crew during the cruise from Port Blair to Barren Island. Captain Pankai Verma is kindly thanked for his support, guidance and the information about the 2000 event. D. James and M. D'Orazio are thanked for providing the major and trace composition of the whole rock by XRF and ICP-MS, respectively. G. Perini, C.M. Petrone and S. Tommasini are warmly thanked for their help during the strontium and neodymium isotopic analysis. R. Poreda and D. Tedesco are thanked for the analysis of the helium isotopic ratio of the fumarolic gas.

Appendix A. Analytical techniques rock specimens

Mineral phase compositions were determined by a JEOL JXA-8600 electron microprobe operating at 15 kV and 15 nA and equipped with a Series II Tracor Northern system. Corrections for matrix effects were made according to the method suggested by Bence and Albee (1968).

Rock samples were crushed with a jaw-crusher, quartered and, eventually, ground in a 250 ml agate mortar ball mill. Major and trace element composition was performed at the University of Edinburgh (Department of Geology) with a Philips PW 1400XRF, using glass disks and pressed pellets, respectively. Reproducibility for most of the trace elements is approximately 1–5 ppm.

Other trace elements, REE and Sr and Nd isotopic determinations were carried on selected samples. Rare Earth Elements (REE), Be, Sc, Co, Cs, Th, U, Ta, Hf were determined by ICP-MS (VG PQII Plus STE) at the University of Pisa (Department of Earth Sciences). Samples were dissolved in PFA vessels on a hot plate at approximately 120 °C with HF+HNO3. The sample solutions (dilution ca. 1:1000) were measured in replicates by external calibration. Analytical precision, evaluated by repeated analysis of the in-house standard HE-1 (Mt. Etna hawaiite), is between 2 and 5% relative standard deviation, except for Gd and Tm (6%) and Be, Sc, and Pb (8%). Sr and Nd isotopic ratios were measured at the University of Florence (Department of Earth Sciences). Sample powder (≈20 mg) was dissolved in a HF–HNO_3–HCl mixture. Sr and Nd fractions were separated following standard chromatographic techniques using AG50×8 and PTFE–HDEHP resins with HCl as eluent. The total procedural blank was <200 pg for Sr and <100 pg for Nd, making blank correction negligible. Mass spectrometric analyses were performed on a Thermo Finnigan Triton–Ti thermal ionization mass spectrometer equipped with nine movable collectors. Sr and Nd isotope compositions were measured in dynamic mode and are reported normalized to $^{86}Sr/^{88}Sr = 0.1194$ and $^{146}Nd/^{144}Nd = 0.7219$, respectively. Exponential-law mass fractionation correction was used for all Sr and Nd isotopic data. Uncertainties in measured (m) and initial (0) isotopic ratios refer to the least significant digits and represent $\pm 2\sigma$ run precision and $\pm 2\sigma$ propagated error, respectively. The external precision of NIST SRM987 was $^{87}Sr/^{86}Sr = 0.710247 \pm 7$ (2σ, $n = 10$), and that of the La Jolla standard was $^{143}Nd/^{144}Nd = 0.511845 \pm 6$ (2σ, $n = 7$) (Avanzinelli et al., 2005).

Appendix B. Fumarolic sample

Fumarolic gas sample was collected with a titanium tube inserted into the gas outlet. The gas phase was conveyed, through pyrex glass dewars, into pre-weighed and pre-evacuated 50 ml thorium-tapped tubes, to which 20 ml of 0.15 M $Cd(OH)_2$ and 4 M NaOH solution had previously been added. The acid gases, viz., CO_2, SO_2, H_2S, HCl, HF, dissolve into the alkaline solutions, H_2O condenses and the unabsorbed gases (N_2, O_2, CO, He, CH_4, Ar, Ne and light hydrocarbons) are collected in the head-space.

In the laboratory, after separation of the liquid and solid phases by centrifugation, the solution was oxidized with H_2O_2, which also allowed SO_3^{2-} to be transformed to SO_4^{2-}, and then SO_2 as SO_4^{2-} was analyzed by ion chromatography (Dionex DX100 ion chromatograph). CdS in the solid phase was dissolved as $CdSO_4$ by oxidation with H_2O_2 and then it was analyzed chromatographically as SO_4^{2-}.

It was followed by extraction of S_8 from residual precipitate with CCl_4, after the dissolution of CdS. The extracted S_8^0 was then oxidized (with I_2 as carrier and $KBrO_3$ as oxidizing agent) in the liquid phase to SO_4^{2-}. SO_4^{2-} was then analyzed by ion chromatography. CO_2 in the caustic solution was analyzed by automatic titration with 0.1 N HCl, while dissolved F^- and Cl^- were analyzed by potentiometer with specific electrode and ion chromatography, respectively (Montegrossi et al., 2001). The gas residual fraction (N_2, H_2, He, O_2, Ar and Ne) was analyzed with a gas chromatography system (Shimadzu 15a) equipped with a thermal conductivity detector. The concentration of CO was determined by a flame ionization detector after conversion to CH_4 at 400 °C. Different hydrocarbon compounds were also analyzed using a Dani 86.10 Gas Chromatograph (Mangani et al., 1991). Analytical precision was <1% for major components and <5% for minor and trace compounds. Colorimetric techniques were used to determine boric acid and ammonium ion contents in the condensate samples using Nessler method. $^{13}C/^{12}C$ ratio of CO_2 (expressed as ‰ PDB) was determined with a Finnigan MAT Delta S mass spectrometer. The CO_2 was purified and dried before analysis following standard procedures (Evans et al., 1988). The reproducibility of δ values for C is ±0.1‰. The $^3He/^4He$ (expressed as R/Ra ratios, where R is the $^3He/^4He$ measured ratio and Ra is the $^3He/^4He$ ratio in the air: 1.39×10^{-6}; Mamyrin and Tolstikhin, 1984) and $^{40}Ar/^{36}Ar$ isotopic ratios were determined using a noble gas mass spectrometer (VG5400), following the procedure of Poreda and Farley (1992).

References

Alam, M.A., Chandrasekharam, D., Vaselli, O., Capaccioni, B., Manetti, P., Santo, A.P., 2004. Petrology of the prehistoric flows and dyke of Barren Island, Andaman Sea, Indian Ocean. In: Proceedings of Indian Academy of Science (Earth and Planetary Science) Special Issue: Magmatism in India through Time, 113, 715–721.

Asimov, P.D., Ghiorso, M.S., 1998. Algorithmic modifications extending MELTS to calculate subsolidus phase relations. American Mineralogist 83, 1127–1131.

Avanzinelli, R., Boari, E., Conticelli, S., Francalanci, L., Guarnieri, L., Perini, G., Petrone, C.M., Tommasini, S., Ulivi, M., 2005. High precision Sr, Nd, and Pb isotopic analyses using the new generetion Thermal Ionisation Mass Spectrometer ThermoFinnigan Triton-Ti®. Periodico di Mineralogia 75 (3), 1–20.

Ball, V., 1888. The volcanoes of Barren and Narcondam Island in the Bay of Bengal. Geological Magazine, 404.

Ball, V., 1893. The volcanoes of Barren and Narcondam Island in the Bay of Bengal. Geological Magazine, 289.

Bandyopadhyay, S., Subramanyam, M.R., Sharma, P.N., 1973. The geology and mineral resources of Andaman and Nicobar Islands. Records of Geological Survey of India 105, 25–68.

Banerjee, B., Shaw, R.K., 2001. Marine magnetic surveys around Barren Island volcano, Anadaman Sea. Current Science 81, 817–818.

Bence, A.E., Albee, A.L., 1968. Empirical factors for the electron microanalyses of silicates and oxides. Journal of Geology 76, 382–483.

Bhatia, S.C., Ravi Kumar, M., Gupta, H.K., 1999. A probabilistic seismic hazard map of India and adjoining regions. Annals of Geophysics 42, 1153–1166.

BGVN, 2005. Lava Flow and Ash Discharges Seen by Coast Guard Personnel on 28 May 2005. Bulletin of Global Volcanic Network, 30:5.

BGVN, 2006. November 2005–January 2006 ash emissions, lava flows, and pyroclastics. Bull. Global Volc. Network, 31:01.

Burns, R.E., 1964. Sea bottom heat flow measurements in the Andaman Sea. Journal of Geophysical Research 69, 4918–4919.

Chandra, U., 1984. Tectonic segmentation of the Burmese–Indonesian Arc. Tectonophysics 105, 279–290.

Chandrasekharam, D., Vaselli, O., Capaccioni, B., Manetti, P., Alam, M.A., 2003. Cold springs of the Barren Island, Andaman Sea, Indian Ocean. Current Science 85, 136–137.

Closs, H., Narain, H., Garde, S.C., 1974. Continental margins of India. In: Burk, C.A., Drake, C.L. (Eds.), The Geology of Continental Margins. Springer-Verlag, New York, pp. 629–639.

Crawford, A.J., Falloon, T.J., Eggins, S., 1987. The origin of island arc high-alumina basalts. Contribution to Mineralogy and Petrology 97, 417–430.

Curray, J.R., Moore, D.G., Lawver, L.A., Emmel, F.J., Raitt, R.W., Henry, M., Kieckhefer, R., 1979. Tectonics of the Andaman Sea and Burma. In: Watkins, J.S., Montadert, L., Dickerson, P.W. (Eds.), American Association of Petroleum Geologists Memoir 1979: Geological and Geophysical Investigations of Continental Margins, vol. 29. pp. 189–198.

Curray, J.R., Emmel, F.J., Moore, D.G., Russel, W.R., 1982. Structure, tectonics, and geological history of the north-eastern Indian Ocean. In: Nairn, A.E., Stheli, F.G. (Eds.), The Ocean Basins and Margins: The Indian Ocean, vol. 6. Plenum, New York, pp. 399–450.

Dasgupta, S., Mukhopadhyay, M., 1993. Seismicity and plate deformation below the Andaman arc, north-eastern Indian Ocean. Tectonophysics 25, 529–542.

Dungan, M.A., Rhodes, J.M., 1978. Residual glasses and melt inclusions in basalts from DSDP legs 45 and 46: evidence for magma mixing. Contributions to Mineralogy and Petrology 67, 417–431.

Eguchi, T., Uyeda, S., Maki, T., 1979. Seismotectonic and tectonic history of the Andaman Sea. Tectonophysics 57, 35–51.

Evans, P., Crompton, W., 1946. Geological factors in gravity interpretation illustrated by evidence from India and Burma. Journal of Geological Society of London 102, 211–249.

Evans, W.C., White, L.D., Rapp, J.B., 1988. Geochemistry of some gases in hydrothermal fluids from the southern Juan de Fuca Ridge. Journal of Geophysical Research 15, 305–313.

Fitch, T.J., 1972. Plate convergence, transcurrent faults and internal deformation adjacent to southeast Asia and the western Pacific. Journal of Geophysical Research 77, 432–4460.

Francke, D., Schnabel, M., Ladage, S., Tappin, D.R., Sönke, N., Djajadihardja, Y., Müller, C., Kopp, H., Gaedicke, C., 2008. The great Sumatra-Andaman earthquakes–Imaging the boundary between the ruptures of the great 2004 and 2005 earthquakes. Earth and Planetary Science Letters 269, 118–130.

Gerbe, M.C., Gourgaud, A., Sigmarsson, O., Harmon, R.S., Joron, J.L., Provost, A., 1992. Mineralogical and geochemical evolution of the 1982–1983 Galunggung eruption (Indonesia). Bulletin of Volcanology 54, 284–298.

Ghiorso, M.S., Sack, R.O., 1995. Chemical mass transfer in magmatic processes: IV. A revised and internally consistent thermodynamic model for the interpolation and extrapolation of liquid–solid equilibria in magmatic system at elevated temperatures and pressures. Contribution to Mineralogy and Petrology 119, 197–212.

Giggenbach, W.F., 1987. Redox processes governing the chemistry of fumarolic gas discharges from White Island, New Zealand. Applied Geochemistry 2, 143–161.

Giggenbach, W.F., 1991. Chemical techniques in geothermal exploration. In: Application of Geochemistry in Geothermal Reservoir Development. UNITAR, New York, pp. 253–273.

Giggenbach, W.F., 1996. Chemical composition of volcanic gases. In: Scarpa, M., Tilling, R.J. (Eds.), Monitoring and Mitigation of Volcanic Hazards. Springer-Verlag, Berlin Heidelberg, pp. 221–256.

Gill, J.B., 1981. Orogenic Andesites and Plate Tectonics. Springer, Berlin. p. 391.

Gupta, H.K., Fleitout, L., Friodevaux, C., 1990. Lithospheric subduction beneath the Arakan Yoma fold belt: quantitative estimates using gravimetric and seismic data. Journal of Geological Society of India 35, 235–250.

Haldar, D., 1989. Petrology and chemistry of recent volcanics of Barren and Narcondam islands the only two recent volcanoes in India. Records of Geological Survey of India 122, 48–49.

Haldar, D., 2001. The current eruption of the Barren Island volcano in the Andaman Sea: a unique phenomenon of the 20th century in the Indian subcontinent. Gondwana Research 4, 629–630.

Haldar, D., Chakraborty, S.C., Chakraborty, P.P., 1999. The 1994–1995 eruption of the Barren Island volcano in the Andaman Sea, India: a resurgent volcanism. Gondwana Geological Magazine (Suppl. 4), 371–384.

Haldar, D., Luhr, J.F., 2003. The Barren Island volcanism during 1991 and 1994–95: eruptive style and lava petrology. Memoirs of the Geological Society of India 52, 313–338.

Haldar, D., Laskar, T., Bandyopadhyay, P.C., Sarkar, N.K., Biswas, J.K., 1992a. The volcanic eruption of the Barren Island volcano, Andaman Sea. Journal of Geological Society of India 39, 411–419.

Haldar, D., Laskar, T., Bandyopadhyay, P.C., Sarkar, N.K., Biswas, J.K., 1992b. A note on the recent eruption of the Barren Island volcano. Indian Minerals 46, 77–88.

Haldar, D., Laskar, T., Bandyopadhyay, P.C., Sarkar, N.K., Biswas, J.K., 1992c. A short account of the on-going eruption of the Barren Island volcano. Records of Geological Survey of India 125, 87–96.

Hobday, J.R., Mallet, F.R., 1885. The volcanoes of Barren and Narcondam islands in the Bay of Bengala. Memoirs of the Geological Survey of India 21, 251–286.

Kohut, E.J., Nielsen, R.L., 2003. Low-pressure phase equilibria of anhydrous anorthite-bearing mafic magmas. Geochemistry Geophysics Geosystems 4, 1–27.

Kuno, H., 1960. High-alumina basalts. Journal of Petrology 1, 121–145.

Luhr, J.F., Haldar, D., 2006. Barren Island volcano (NE Indian Ocean): island–arc high-alumina basalts produced by troctolite contamination. Journal of Volcanology and Geothermal Research 149, 177–212.

Mallet, F.R., 1895. Some early allusions to Barren island: with a few remarks thereon. Records of the Geological Survey of India Memoir 28 (1), 22–34.

Mamyrin, B.A., Tolstikhin, I.N., 1984. Helium isotopes in nature. In: Fyfe, W.S. (Ed.), Development in Geochemistry. Elsevier, Amsterdam, pp. 1–273.

Mangani, F., Cappiello, A., Capaccioni, B., Martini, M., 1991. Sampling and analyses of light hydrocarbons in volcanic gases. Chromatographia 32, 441–444.

Marsh, B.D., Fournelle, J., Myers, J.D., Chou, I.M., 1990. On plagioclase thermometry in island arc rocks: experiments and theory. In: Spencer, R.J., Chou, I.M. (Eds.), Fluid-Mineral Interactions: A Tribute to H.P. Eugster, vol. 2. Geochemical Society Special Publication, pp. 65–83.

McDonough, W.F., Sun, S.S., 1995. The composition of the earth. Chemical Geology 120, 223–253.

Maury, R.C., Pubellier, M., Rangin, C., Wulput, L., Cotton, J., Socquet, A., Bellon, H., Guillaud, J-Ph., Htun, H.M., 2004. Quaternary calc-alkaline and alkaline volcanism in an hyper-oblique convergence setting central Myanmar and western Yunnan. Bulletin de la Societe Geologique de France 175, 461–472.

Mitchell, A.H.G., 1985. Collision-related fore-arc and back-arc evolution of the Northern Sunda Arc. Tectonophysics 116, 323–334.

Montegrossi, G., Tassi, F., Vaselli, O., Buccianti, A., Garofalo, K., 2001. Sulfur species in volcanic gases. Analytical Chemistry 73, 3709–3715.

Mukhopadhyay, M., 1984. Seismotectonics of subduction and back-arc rifting under the Andaman Sea. Tectonophysics 108, 229–239.

Mukhopadhyay, M., Dasgupta, S., 1988. Deep structure and tectonics of the Burmese arc: constraints from earthquake and gravity data. Tectonophysics 149, 299–322.

Mukhopadhyay, M., Krishna, M.R., 1991. Gravity field and deep structure of the Bengal Fan and its surrounding continental margins, northeast Indian Ocean. Tectonophysics 186, 365–386.

Ni, J.F., Speziale, M.G., Bevis, M., Holt, W.E., Wallace, T.C., Seager, W.R., 1989. Accretionary tectonics of Burma and the three dimensional geometry of the Burma subduction. Geology 17, 68–71.

Pal, T., Bandopadhyay, P.C., Mitra, S.K., Raghav, S.R., 2007a. Recent eruption (2005) of Barren volcano: an explosive inner arc volcanism in Andaman Sea. Journal of the Geological Society of India 69, 1195–1202.

Pal, T., Mitra, S.K., Sengupta, S., Katari, A., Bandopadhyay, P.C., Bhattacharya, A.K., 2007b. Dacite–andesites of Narcondam volcano in the Andaman Sea – an imprint of magma mixing in the inner arc of the Andaman–Java subduction system. Journal of Volcanology and Geothermal Research 168, 93–113.

Peccerillo, A., Taylor, S.R., 1976. Geochemistry of Eocene calc-alkaline rocks from Kastamonu area, Northern Turkey. Contribution to Mineralogy and Petrology 58, 63–81.

Plank, T., Langmuir, C.H., 1998. The chemical composition of subducting sediment and its consequences for the crust and mantle. Chemical Geology 145, 325–394.

Poreda, R.J., Farley, K.A., 1992. Rare-gases in Samoan xenoliths. Earth and Planetary Science Letters 113, 129–144.

Raina, V.K., 1987. A note on sulphur occurrence in the volcanoes of the Bay of Bengal. Indian Minerals 41, 79–86.

Ravi Shankar, Haldar, D., Absar, A., Chakraborty, S.C., 2001. Pictorial Monograph of Barren Island Volcano: the Lone Active Volcano in the Indian Subcontinent. Geological Survey of India Special Publication No. 67, pp. 88.

Rodolfo, K.S., 1969. Bathymetry and marine geology of the Andaman basin and tectonic implications for southeast Asia. Geological Society of America Bulletin 80, 1203–1230.

Shock, L.E., 1993. Hydrothermal dehydration of aqueous organic compounds. Geochimica et Cosmochimica Acta 57, 3341–3349.

Siebert, L., Simkin, T., 2002. Volcanoes of the world: an illustrated catalog of Holocene volcanoes and their eruptions. In: Proceedings of the Global Volcanism program Digital Information Series, Smithsonian Institution, GVP-3. <http://www.volcano.si.edu/gvp/world/>.

Simkin, T., Siebert, L., 1994. Volcanoes of the world. Geoscience Press, Tucson. 249p.

Sisson, T.W., Grove, T.L., 1993. Experimental investigations of the role of H_2O in calcalkaline differentiation and subduction zone magmatism. Contribution to Mineralogy and Petrology 113, 143–166.

Stolz, A.J., Varne, S., Davies, G.R., Wheller, G.E., Foden, J.D., 1990. Magma source component in an arc-continent collision zone: the Flores–Lembata sector, Sunda arc, Indonesia. Contribution to Mineralogy and Petrology 105, 585–601.

Stormer, J.C., Nicholls, J., 1978. XLFRAC a programme for interactive testing of magmatic differentiation models. Computers and Geosciences 4, 143–159.

Sun, S.S. and McDonough, W.F., 1989. Chemical and isotopic systematics of oceanic basalts: implications for mantle composition and processes. In: Saunders, A.D., Norry, M.J. (Eds.), Magmatism in Ocean Basins. Geological Society of London, Special Publications No. 42, pp. 313–334.

Symonds, R.B., Gerlach, T.M., Reed, M.H., 2001. Magmatic gas scrubbing: implications for volcano monitorino. Journal of Volcanology and Geothermal Research 108, 303–341.

Turner, S., Foden, J., 2001. U, Th and Ra disequilibria, Sr, Nd and Pb isotope and trace element variations in Sunda arc lavas: predominance of a subducted sediment component. Contribution to Mineralogy and Petrology 142, 43–57.

Uyeda, S., Kanamori, H., 1979. Back-arc opening and the mode of subduction. Journal of Geophysical Research 84, 1049–1061.

Verma, R.K., Mukhopadhyay, M., Ahluwalia, M.S., 1976. Earthquake mechanisms and tectonics of Northern Burma. Tectonophysics 32, 387–399.

Washington, H.S., 1924. The lavas of Barren and Narcondam Islands. American Journal of Sciences 7 (5th series), p. 22.

Wilson, M., 1989. Igneous Petrogenesis: A Global Tectonic Approach. Harper Collins Ed., pp. 466.

Wheller, G.E., Varne, R., Foden, J.D., Abbott, M.J., 1987. Geochemistry of Quaternary volcanism in the Sunda-Banda arc, Indonesia, and three-component genesis of island–arc basaltic magmas. Journal of Volcanology and Geothermal Research 32, 137–160.

Yoder, H.S., 1969. Calcalkalic andesites: experimental evidence bearing on the origin of their assumed characteristics. In: McBirney, A.R. (Ed.), Proceedings of Andesite Conference, Oregon Department of Geology and Mineral Industries Bulletin, vol. 65. pp. 77–89.